International Journal of Nanomedicine

Dovepress
open access to scientific and medical research

Open Access Full Text Article

ORIGINAL RESEARCH

Differential nanoreprotoxicity of silver nanoparticles in male somatic cells and spermatogonial stem cells

This article was published in the following Dove Press journal:
International Journal of Nanomedicine
16 February 2015
Number of times this article has been viewed

Xi-Feng Zhang*
Yun-Jung Choi*
Jae Woong Han
Eunsu Kim
Jung Hyun Park
Sangiliyandi Gurunathan
Jin-Hoi Kim

Department of Animal Biotechnology, Konkuk University, Seoul, South Korea

*These authors contributed equally to this work

Background: Silver nanoparticles (AgNPs) possess unique physical, chemical, and biological properties. AgNPs have been increasingly used as anticancer, antiangiogenic, and antibacterial agents for the treatment of bacterial infections in open wounds as well as in ointments, bandages, and wound dressings. The present study aimed to investigate the effects of two different sizes of AgNPs (10 nm and 20 nm) in male somatic Leydig (TM3) and Sertoli (TM4) cells and spermatogonial stem cells (SSCs).

Methods: Here, we demonstrate a green and simple method for the synthesis of AgNPs using *Bacillus cereus* culture supernatants. The synthesized AgNPs were characterized using ultraviolet and visible absorption spectroscopy, X-ray diffraction, Fourier transform infrared spectroscopy, and transmission electron microscopy (TEM). The toxicity of the synthesized AgNPs was evaluated by the effects on cell viability, metabolic activity, oxidative stress, apoptosis, and expression of genes encoding steroidogenic and tight junction proteins.

Results: AgNPs inhibited the viability and proliferation of TM3 and TM4 cells in a dose- and size-dependent manner by damaging cell membranes and inducing the generation of reactive oxygen species, which in turn affected SSC growth on TM3 and TM4 as feeder cells. Small AgNPs (10 nm) were more cytotoxic than medium-sized nanoparticles (20 nm). TEM revealed the presence of AgNPs in the cell cytoplasm and nucleus, and detected mitochondrial damage and enhanced formation of autosomes and autolysosomes in the AgNP-treated cells. Flow cytometry analysis using Annexin V/propidium iodide staining showed massive cell death by apoptosis or necrosis. Real-time polymerase chain reaction and western blot analyses indicated that in TM3 and TM4 cells, AgNPs activated the p53, p38, and pErk1/2 signaling pathways and significantly downregulated the expression of genes related to testosterone synthesis (TM3) and tight junctions (TM4). Furthermore, the exposure of TM3 and TM4 cells to AgNPs inhibited proliferation and self-renewal of SSCs.

Conclusion: Our results suggest that AgNPs exhibit size-dependent nanoreprotoxicity in male somatic cells and SSCs, strongly suggesting that applications of AgNPs in commercial products must be carefully evaluated. Further studies of AgNPs-induced nanoreprotoxicity in animal models are required.

Keywords: Sertoli cells, Leydig cells, apoptosis, oxidative stress, tight junction proteins, apoptosis

Correspondence: Sangiliyandi Gurunathan/Jin-Hoi Kim
Department of Animal Biotechnology, Konkuk University, Seoul 143-701, South Korea
Tel +82 2 450 3687
Fax +82 2 544 4645
Email gsangiliyandi@yahoo.com/ jhkim541@konkuk.ac.kr

Introduction

Nanomaterials are becoming extremely popular as biological, therapeutic, medical, and antimicrobial agents, and also as transfection vehicles and fluorescent tags. Compared to conventional materials, nanoparticles exhibit unique electrical, light-emitting, and catalytic properties.[1] Silver nanoparticles (AgNPs) have recently gained popularity and are widely used in textile and food industries, cosmetics, pharmaceutical products,

electronics, paints, and construction materials.[2,3] The small size of AgNPs (1–100 nm) enhances their physical, chemical, magnetic, and optical properties.[4,5] In addition, AgNPs have become one of the most common nanomaterials used as antimicrobial agents and disinfectants in medicine and industry[4,5] because they exhibit significant activity against both Gram-negative and Gram-positive bacteria and viruses.[6–8] The investigation of bactericidal activity of nanomaterials is intensifying because of the emergence of new drug-resistant bacterial strains.

As an inevitable consequence of the rapid increase in AgNPs manufacturing and utilization, there is a danger of potential toxic effects. AgNPs can enter the human gastrointestinal tract by several routes, including air, water, food, or soil and can be distributed throughout the body via the circulatory system.[9–11] Oral administration of AgNPs to male rats caused significant decreases in body weight and dose-dependent changes in alkaline phosphatase activity and cholesterol levels, resulting in slight liver damage.[12,13] AgNPs were found in various body tissues, including the blood, brain, liver, spleen, kidneys, thymus, lungs, and heart.[14–19] Previous studies have demonstrated that AgNPs can exert cytotoxic and genotoxic effects both in vitro (human cell lines[20–25]) and in vivo (mice[26,17] and fish[27,28]).

Oxidative stress can strongly affect testicular functions important for spermatogenesis.[29] Reactive oxygen species (ROS) are generated either by the mitochondrial electron transport chain or by nicotinamide adenine dinucleotide phosphate oxidase.[30] Mitochondrial-derived ROS have been implicated in a number of diseases and are known to cause cell and tissue destruction through DNA damage, lipid peroxidation, protein oxidation, and carbonylation, depletion of cellular thiols, and activation of proinflammatory cytokine release.[30,31] Excessive production of ROS induces cellular apoptosis via activation of the p38 mitogen-activated kinase (MAPK)-p16 and HSP70-JNK/c-Jun pathways.[32,33]

The aims of this study were to perform the synthesis of differently sized (10 and 20 nm) AgNPs using *Bacillus cereus* culture supernatant and to examine AgNPs potential toxicity for the cells involved in spermatogenesis, such as somatic Leydig (TM3) and Sertoli (TM4) cells and spermatogonial stem cells (SSCs) derived from prepubertal BALB/c mouse testes. In addition, we investigated the mechanisms involved in AgNPs-induced toxicity.

Materials and methods

Bacterial strains and reagents

Luria-Bertani (LB) agar was purchased from USB Corporation (Santa Clara, CA, USA). Mueller Hinton broth and agar, silver nitrate, and crystal violet were purchased from Sigma-Aldrich (St Louis, MO, USA). All other chemicals were purchased from Sigma-Aldrich unless otherwise stated. *B. cereus* strains were maintained in our culture collection.

Synthesis and characterization of AgNPs

A characterized *B. cereus* (GenBank accession number KF944447) isolate was inoculated into flasks containing sterile LB broth and incubated for 24 hours at 37°C with agitation (200 rpm). After incubation, the culture was centrifuged at 10,000 rpm for 10 minutes and the supernatant was used for AgNP synthesis. In a typical reaction, culture supernatant was mixed with 1 mM and 5 mM aqueous silver nitrate ($AgNO_3$) solution and incubated at 60°C for 6 hours to produce AgNPs of two different sizes (10 and 20 nm). The synthesized particles were characterized as previously described.[34] X-ray diffraction (XRD) analyses were performed using an X-ray diffractometer (Bruker D8 DISCOVER; Bruker AXS GmBH, Karlsruhe, Germany). The high-resolution XRD measurements were performed at 3 kW with Cu target using a scintillation counter (λ=1.5406 Å) at 40 kV and 40 mA, and were recorded in the range of 2θ=5° to 80°. Further characterization of AgNPs surface changes and composition was performed by Fourier transform infrared spectroscopy (FTIR) (PerkinElmer Spectroscope GX; PerkinElmer, Waltham, MA, USA). Transmission electron microscopy (TEM) (Hitachi H-7500; Seoul National University, Seoul, South Korea) was used to determine AgNPs size and morphology. TEM images of bio-AgNPs were obtained at an accelerating voltage of 300 kV.[35]

Cell culture and treatment with AgNPs

TM3 (KCLB No 21714) and TM4 (KCLB No 21715) cell lines were obtained from Korean cell line bank (Seoul, South Korea). TM3 and TM4 cells were cultured in Dulbecco's Modified Eagle's Medium (DMEM) (Hyclone, Logan, UT, USA) supplemented with 10% fetal bovine serum (FBS), 100 U/mL penicillin, and 100 µg/mL streptomycin at 37°C in a 5% CO_2 atmosphere. Cells were seeded onto 6-well plates at a density of 1×10^4 cells per well and incubated for 24 hours prior to experiments. The cells were washed with phosphate-buffered saline (PBS; pH 7.4) and incubated in fresh medium containing different concentrations of AgNPs prepared in water.

Animals

BALB/c mice were housed in wire cages at 22°C±1°C with 70% humidity under a 12/12-hour light–dark cycle. Animals

had access to food and water ad libitum. All experiments were performed with approval from the Institutional Animal Care and Use Committee at Konkuk University (IACUC approval number KU11035; Seoul, South Korea).

Preparation and culture of SSCs

SSCs were cultured in SSC media (SSCM) based on α-minimum essential medium supplemented with 10% FBS, 1% 100× glutamine, 1% noncanonical amino acid, 1% penicillin-streptomycin, 0.5% mercaptoethanol, 0.01 mM sodium pyruvate, 100 μg/mL transferrin, 25 μg/mL insulin, 10 μg/mL putrescine, 0.1 μg/mL GDNF, and 20 μg/mL epidermal growth factor. High-glucose DMEM supplemented with 10% FBS and 1% penicillin-streptomycin was used for feeder cells.

Testes were collected from 21-day-old male imprinting control region mice. Two-step enzymatic digestion was used to treat cell suspension in SSCM at 37°C in a 5% CO_2 humidified incubator. After 24 hours of culture, nonadherent SSCs were collected and transferred to new dishes coated with mouse embryonic fibroblasts as feeder cells, where they proliferated for 7 days. SSCs were verified using polymerase chain reaction (PCR), immunochemistry, and fluorescence-activated cell sorting (FACS).

TM3 and TM4 cells were collected by centrifugation, resuspended in warm feeder cell medium, and plated in 12-well culture dishes precoated with 0.2% gelatin at the concentration of 8×10^4 cells. The feeder cells were cultured for 24 hours and inactivated with 12 μg/mL of mitomycin C for 2.5 hours. After washing with Dulbecco's PBS three times, SSCM without or with 10 μg/mL of AgNPs was added for 24 hours. Culture supernatant was then collected, centrifuged for 15 minutes at 15,000 rpm to remove the nanoparticles, mixed with fresh SSCM (1:1), and added for 72 hours to fresh SSCs cultured on TM3 or TM4 cells as feeder cells. SSCs were then collected and analyzed for gene expression; alternatively, all cells (SSCs and feeder cells) were collected to measure the proliferation of SSCs.

Cytotoxicity assay

Cell counting kit-8 (CCK-8) assay

Typically, 1×10^4 cells were seeded in a 96-well plate and cultured in DMEM supplemented with 10% FBS at 37°C under 5% CO_2 in a humidified incubator for 24 hours. Then, fresh medium containing various concentrations of AgNPs was added for another 24 hours. Cell viability was assessed by adding 10 μL of CCK-8 solution (Dojindo Laboratories, Kumamoto, Japan) to each well for 3 hours at 37°C, and the absorbance was measured at 450 nm using a microplate reader (PerkinElmer). To correct for background absorbance, cell-free medium-containing wells were used as control, and the average absorbance of the control wells was subtracted from that of the other wells.

MTS assay

Cell viability was also measured using the 3-(4, 5-dimethylthiazol-2-yl)-5-(3-carboxymethoxyphenyl)-2-(4-sulfophenyl)-2H-tetrazolium, inner salt (MTS) assay. Cells were plated as above for 24 hours, washed twice with 100 μL of serum-free DMEM, and incubated with 100 μL of AgNP suspensions at various concentrations in serum-free DMEM. After 24-hour exposure, the cells were washed twice with serum-free DMEM, and MTS reagent was added to each well containing 100 μL of serum-free DMEM. After 1-hour incubation at 37°C under 5% CO_2, 80 μL of the mixture was transferred to another 96-well plate, and the absorbance was measured at 490 nm. Cell viability (%) of the treated cells was determined relative to that of control cells set as 100%. The results are presented as the mean ± standard deviation (SD) of three independent experiments.

Lactate dehydrogenase (LDH) assay

TM3 and TM4 cells were pretreated with 10 mM N-acetyl L-cysteine (NAC) (Sigma-Aldrich) for 1 hour and then exposed to AgNPs for 12 hours. Cell membrane integrity was evaluated by determining LDH activity in culture supernatant according to the manufacturer's instructions (LDH Assay kit; Abcam, Cambridge, UK). The LDH assay is based on the leakage of the cytosolic LDH from cells with damaged cellular membranes. In our experiments, AgNP-induced cytotoxicity was quantitatively monitored by measuring LDH activity in the supernatant.

Measurement of ROS

Intracellular ROS concentrations were measured using the oxidation-sensitive fluoroprobe 2,7-dichlorodihydrofluorecein diacetate (H2DCF-DA) (Thermo Fisher Scientific, Waltham, MA, USA) with some modifications. Briefly, TM3 and TM4 cells were pretreated with 10 mM NAC for 1 hour and exposed to AgNPs at half maximal inhibitory concentration (IC_{50}), 0.5% dimethyl sulfoxide (DMSO) (negative control), or 50 μM hydrogen peroxide (H_2O_2) (positive control) for 12 hours. Next, 10 μM 2-7-dichlorofluorescein diacetate (Sigma-Aldrich) was added to the cells for 1 hour, and the formation of the fluorescent 2′,7′-dichlorofluorescein (DCF), an indicator of ROS generation,

was measured using a spectrofluorometer (excitation at 480 nm, emission at 530 nm).

Cellular uptake of AgNPs

Ultrathin cell sections were analyzed using TEM to determine the intracellular distribution of AgNPs. Briefly, the cells were treated with AgNPs for 24 hours, washed two times with phosphate buffer to remove excess unbound nanoparticles, fixed in 2.5% glutaraldehyde for 2 hours, dehydrated in an ethanol series, and embedded in epoxy resin. Cellular morphological characteristics and intracellular AgNPs distribution and agglomeration were investigated by TEM of ultrathin sections placed on grids.[20]

Flow cytometry analysis

AgNPs-induced apoptosis was analyzed using the Alexa Fluor® 488 Annexin V/Dead Cell Apoptosis Kit (Thermo Fisher Scientific). Cells were pretreated with 10 mM NAC for 1 hour, incubated with AgNPs for 6 hour, and stained with Annexin V and propidium iodide for flow cytometry analysis.

RNA extraction and real-time PCR

Total RNA was prepared using the RNeasy Mini Kit (Qiagen, Venlo, the Netherlands) according to the manufacturer's protocol. Reverse transcription was performed using the QuantiTect® Reverse Transcription kit (Qiagen), and quantitative real-time PCR (RT-PCR) was performed using Maxima SYBR Green/ROX qPCR Master Mix (Thermo Fisher Scientific) according to the manufacturers' instructions. Primers are shown in Table 1. The expression of each gene was analyzed in triplicate and normalized to that of β-actin used as a housekeeping gene. The expression level was evaluated by the $2^{-\Delta\Delta Ct}$ method.

Western blot analysis

The cells were treated as above, harvested, washed with ice-cold PBS, and lysed with ice-cold RIPA lysis buffer. Protein concentrations were measured using the BCA Protein Assay Reagent (Pierce, Rockford, IL, USA). Equivalent amounts of protein were separated by sodium dodecyl sulfate-polyacrylamide electrophoresis in 8%–12% gels and transferred to polyvinylidene difluoride membranes (Millipore Corp., Billerica, MA, USA). The membranes were blocked with 6% nonfat dry milk at room temperature for 1 hour, and incubated with the primary antibodies overnight at 4°C. The following primary antibodies were used: anti-Bax (ab10813; Abcam), anti-Bcl-2 (ab7973; Abcam), anti-p-Erk1/2 (Thr202/Tyr204) (sc-16982; Santa Cruz Biotechnology, Dallas, TX, USA), anti-p-p38 (sc-7973; Santa Cruz Biotechnology), anti-P-p53 (S15) (12571S; Cell Signaling, Danvers, MA, USA), anti-RAD51 (ab88572; Abcam), and anti-β-actin (ab8227; Abcam). The membranes were washed and incubated with horseradish peroxidase-conjugated secondary antibodies at room temperature for 1 hour. Blots were developed using enhanced chemiluminescence.

Statistical methods

The data are presented as the mean ± SD of at least three independent experiments. Differences between the means were tested by Student's *t*-test or one-way analysis of variance (ANOVA) followed by Tukey's test for multiple comparisons using the Graph-Pad Prism software. The differences were considered significant at $P<0.05$.

Results and discussion

Characterization of biologically synthesized AgNPs

The aim of this experiment was to produce small AgNPs of two different sizes using *B. cereus* culture supernatant and to evaluate their cytotoxic effects in somatic TM3 and TM4 cells and SSCs. To produce AgNPs of two different sizes of AgNPs, 1 mM and 5 mM, $AgNO_3$ was added to *B. cereus* culture supernatant and incubated at 60°C, pH 8.0, for 6 hours. As a result, AgNPs of 10 nm and 20 nm were obtained from 5 mM and 1 mM $AgNO_3$, respectively, and characterized as previously described[34] using analytical techniques, including ultraviolet and visible spectroscopy, which is one of the most widely used methods for structural characterization of AgNPs.[36,37] The absorption spectra of 10 nm and 20 nm AgNPs showed highly symmetric single-band absorption, with peak maxima at 410 nm (Figure 1A) and 395 nm (Figure 1B), respectively, indicating excitation of surface plasmons typical for AgNPs.[34] In the ultraviolet and visible spectrum, a strong broad peak was observed between 395 and 410 nm, indicating AgNPs formation. The specific features of this peak can be attributed to surface plasmons and have been well documented for various metal nanoparticles with sizes ranging from 2 nm to 100 nm.[36,38] A blue shift indicates a reduction in the mean diameter of AgNPs. A surface plasmon resonance band was observed to be blue-shifted and to have a sharp, narrow shape, indicating the formation of spherical and homogeneously distributed AgNPs. Similarly, Khalil et al[39] have reported that as the concentration of olive leaf extract increased, the absorption

Table 1 Primers used for quantitative real-time polymerase chain reaction

Genes	Sequences of primers	GenBank
Gapdh	F: 5′-AGGTCGGTGTGAACGGATTTG-3′	NC_000072.6
	R: 5′-TGTAGACCATGTAGTTGAGGTCA-3′	
Atg6	F: 5′-GGCCAATAAGATGGGTCTGA-3′	NC_000077.6
	R: 5′-GCTGCACACAGTCCAGAAAA-3′	
Atg7	F: 5′-CAGTAGCCTGTAGAATAAC-3′	NC_000072.6
	R: 5′-GTAGGTGTGTCTGTAATC-3′	
Atg8	F: 5′-CGGCTTCCTGTACATGGTTT-3′	NC_000074.6
	R: 5′-ATGTGGGTGCCTACGTCTC-3′	
Cx43	F: 5′-TGTGGGCAAGACACGAATATG-3′	NC_000076.6
	R: 5′-GACAAGGTCCAAGCCTACTCCC-3′	
Cyp17a1	F: 5′-TGACCAGAAACTGGAGAAGATGATA-3′	NC_000085.6
	R: 5′-CCTTGTTCTCAAAAGAGATGTTGAA-3′	
Cyp19a1	F: 5′-GGAAGTGCCTGCAACTACTACAATA-3′	NC_000075.6
	R: 5′-TTGTTGTTAAATATGATGCCGTTCT-3′	
Caspase-3	F: 5′-GATAATGTCTTAGAACTTGAATCC-3′	NC_000074.6
	R: 5′-CTTCCATAAATCAGGTCCAA-3′	
Caspase-8	F: 5′-GAGTTGCCACCTTCAGTT-3′	NC_000067.6
	R: 5′-TCACTGTCTTGTTCTCTTGG-3′	
Caspase-9	F: 5′-GACTTACAAGCAGATTCC-3′	NC_000070.6
	R: 5′-AGAATAATGAGGCAGAGA-3′	
3β-Hsd	F: 5′-CTGAATGTTACTGGCAAATTCTC-3′	NC_000069.6
	R: 5′-TGTTGGACGCAGCAGGAAAAAA-3′	
17β-Hsd	F: 5′-GTTCTCGCAGCACCTTTTTC-3′	NC_000077.6
	R: 5′-AAATCTTCACACCGCTTCCC-3′	
StAR	F: 5′-AGAGCTCAACTGGAGAGCACTG-3′	NC_000074.6
	R: 5′-AGCCTTCCTGGTTGTTGAGTATG-3′	
ZO-1	F: 5′-CTCTGGTGGAAGAGATAATCCTCA-3′	NC_000073.6
	R: 5′-GTTTTTCCCACTCTTCCTTAGCTG-3′	
Claudin-11	F: 5′-GTCACAACGTCCACCAATGACT-3′	NC_000069.6
	R: 5′-AGAACTGTCAACAGCAGCAAGAT-3′	
Amh	F: 5′-GGATGACTCCCACCCTGGTG-3′	NC_000076.6
	R: 5′-GGGAAAGGCATGGTGTCCAG-3′	
Ar	F: 5′-TGCCTCCGAAGTGTGGTATC-3′	NC_000086.7
	R: 5′-CCGTAGTGACAGCCAGAAGC-3′	
LhR	F: 5′-TTTTCCAAACAATGTGAAAHCA-3′	NC_000083.6
	R: 5′-CAGGGATTGAAAGCATCTGG-3′	
Cyp11a1	F: 5′-AAGGTGTAGCTCAGGACTTCATCA-3′	NC_000075.6
	R: 5′-GTGGAACATCTGGTAGACAGCATT-3′	
Tgfβ1	F: 5′-CGAAGCGGACTACTATGCTAAAGA-3′	NC_000073.6
	R: 5′-CATGTTGCTCCACACTTGATTTTA-3′	
Vimentin	F: 5′-TTTGCCAACTACATCGACAAGGT-3′	NC_000068.7
	R: 5′-CATCTCCTCCTGCAATTTCTCTC-3′	
Oct4	F: 5′-GGCGTTCTCTTTGGAAAGGTGTTC-3′	NC_000083.6
	R: 5′-CTCGAACCACATCCTTCTCT-3′	
Nanog	F: 5′-TTACAAGGGTCTGCTACTGAGATG-3′	NC_000072.6
	R: 5′-TGCTTATAGCTCAGGTTCAGAATG-3′	
Rex-1	F: 5′-GGCCAGTCCAGAATACCAGA-3′	NC_000074.6
	R: 5′-GAACTCGCTTCCAGAACCTG-3′	
Tex-18	F: 5′-TGTCCAGGTGAGCACTTCAG-3′	NC_000076.6
	R: 5′-TCTTCCTGAGCACACCCTCT-3′	
Vasa	F: 5′-TGGCAGAGCGATTTCTTTTT-3′	NC_000079.6
	R: 5′-CGCTGTATTCAACGTGTGCT-3′	
Zbtb16	F: 5′-ACCAGTGTACCATCTGCACG-3′	NC_000075.6

(*Continued*)

Table 1 (*Continued*)

Genes	Sequences of primers	GenBank
	R: 5′-CTGCTCTACCATGTGTTGGG-3′	
Gdnf	F: 5′-GTTAATGTCCAACTGGGGGTCTAC-3′	NC_000081.6
	R: 5′-CGCTTCGAGAAGCCTCTTACC-3′	
Stra8	F: 5′-CTCCTCCTCCACTCTGTTGC-3′	XM_004046 273
	R: 5′-GCGGCAGAGACAATAGGAAG-3′	
Dazl	F: 5′-TGACGTGGATGTGCAGAAGAT-3′	NM_010021
	R: 5′-AGGAGGATATGCCTGAACATACT-3′	
Sycp3	F: 5′-CCGCTGAGCAAACATCTAAAG-3′	NC_000076
	R: 5′-ATCAGCAACATCTTCTTCTGAACC-3′	
c-Kit	F: 5′-CGTGAACTCCATGTGGCTAA-3′	NC_000071.6
	R: 5′-CGTCTCCTGGCGTTCATAAT-3′	
Pcna	F: 5′-CGTCTCCTTGGTACAGCTTACTCT-3′	NC_000068.7
	R: 5′-TGCATTATCTTCAGCCCTTAATGT-3′	
Etv5	F: 5′-CTTGGTTAGCTGAAGCACAAGTTC-3′	NC_000082.6
	R: 5′-TTCTCCATACTTAGCACCAAGAGC-3′	
Bcl6	F: 5′-GACGTGCTTAGCAATCTGAATGAG-3′	NC_000077.6
	R: 5′-ATGAAGTCCAGAAGAGGAGCAAAG-3′	

Abbreviations: F, forward; R, reverse.

peak sharply increased, and a blue shift was observed from 458 nm to 441 nm. Gurunathan et al[34] have shown that $AgNO_3$ concentration, temperature, and pH play important roles in determining the size of AgNPs.

XRD analysis of AgNPs

Further characterization was performed to confirm the crystalline nature of AgNPs. XRD spectra for both 10 and 20 nm AgNPs showed three intense peaks in the whole spectrum of 2θ values, ranging from 20° to 50° (Figure 2). A comparison of our XRD spectra with the standard confirmed that the AgNPs formed in our experiments were nanocrystals, as evidenced by the peaks at 2θ values of 28.8°, 31.9°, and 46°, corresponding to the 111, 200, and 222 planes for silver, respectively (Figure 2). XRD data confirmed that AgNPs exhibited 2θ values corresponding to those previously

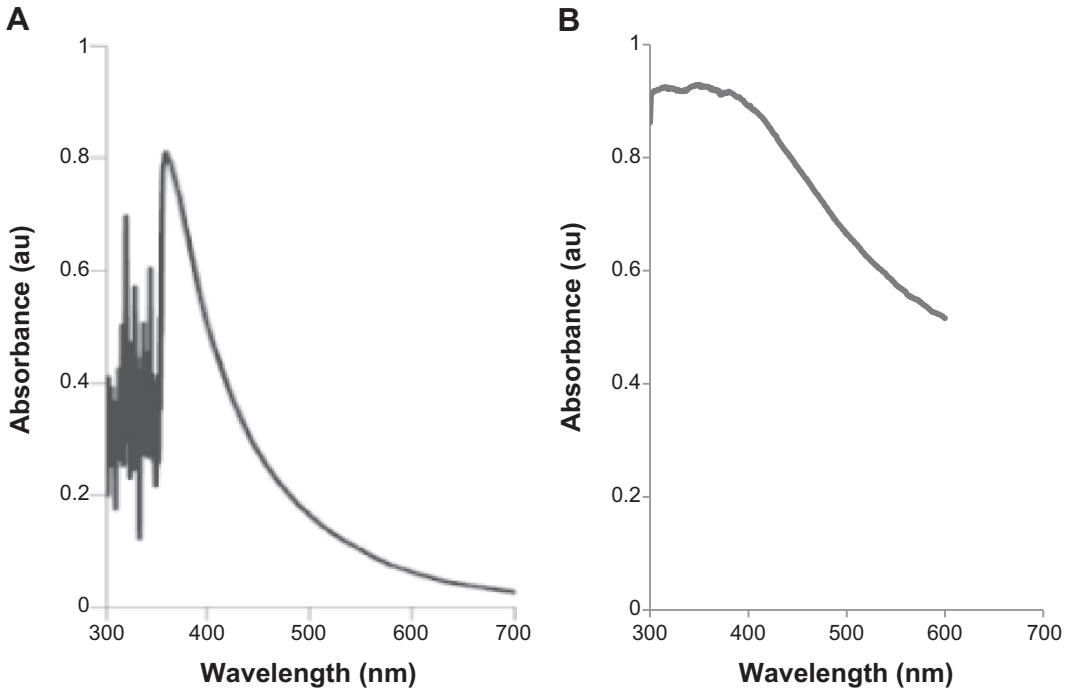

Figure 1 Synthesis and characterization of AgNPs.
Notes: The absorption spectra of 10 nm (**A**) and 20 nm (**B**) AgNPs exhibited strong broad peaks at 395 nm and 410 nm, respectively.
Abbreviations: AgNPs, silver nanoparticles; au, absorbance units.

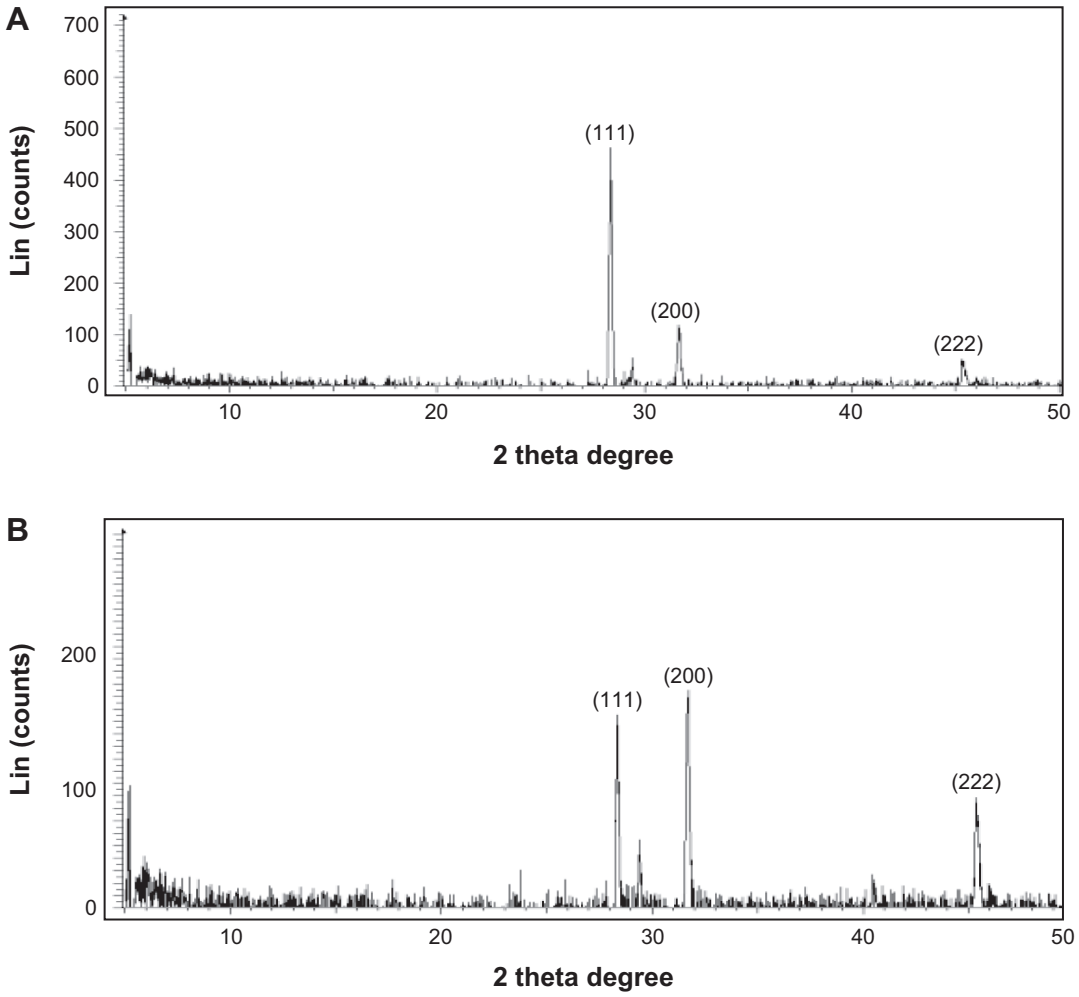

Figure 2 XRD spectra of AgNPs.
Notes: X-ray diffraction (XRD) spectra of AgNPs of 10 nm (**A**) and 20 nm (**B**); there are three intense peaks across the spectrum of 2θ values ranging from 20° to 50°.
Abbreviation: AgNPs, silver nanoparticles.

reported for silver nanocrystals prepared from culture supernatants of *Bacillus licheniformis*[38] and *Escherichia coli*. The diffraction peaks of the (111), (200), and (222) lattice planes appeared in the XRD spectra of AgNPs. Thus, the observed XRD patterns corresponded to the crystalline planes of face-centered-cubic AgNPs, suggesting that the obtained AgNPs had crystalline nature.

FTIR spectra of AgNPs

FTIR spectra were used to identify the presence of biomolecules that could potentially contribute to the reduction of Ag^+ ions or capping of the bioreduced AgNPs.[40,41] Previous studies have proposed that protein–nanoparticle interactions can occur either through free amine groups or cysteine residues in proteins and via electrostatic attraction of negatively charged carboxylate groups in some enzymes.[37,42] The two bands observed at 1,380 cm^{-1} and 1,030 cm^{-1} can be assigned to the C–N stretching vibrations of the aromatic and aliphatic amines, respectively.[43] Figure 3A and B shows FTIR spectra of AgNPs synthesized from bacterial supernatant, with peaks at 3,430 cm^{-1} and 1,650 cm^{-1} characteristic of the stretching modes for the O–H and C=O groups. AgNPs of different sizes showed similar spectra without any significant differences. These observations indicate protein binding to AgNPs, which can lead to their stabilization. However, it is important to note that protein size, shape, and conformation play an important role in the reaction with nanoparticles.[37]

Analysis of AgNP size and surface morphology by TEM

TEM is one of the most effective methods to analyze the size and morphology of nanoparticles.[41] TEM micrographs of both types of AgNPs (10 nm and 20 nm) revealed distinct, uniformly spherical particles well separated from each other. The average particle size was estimated based on the measurements of more than 300 particles; it was calculated in

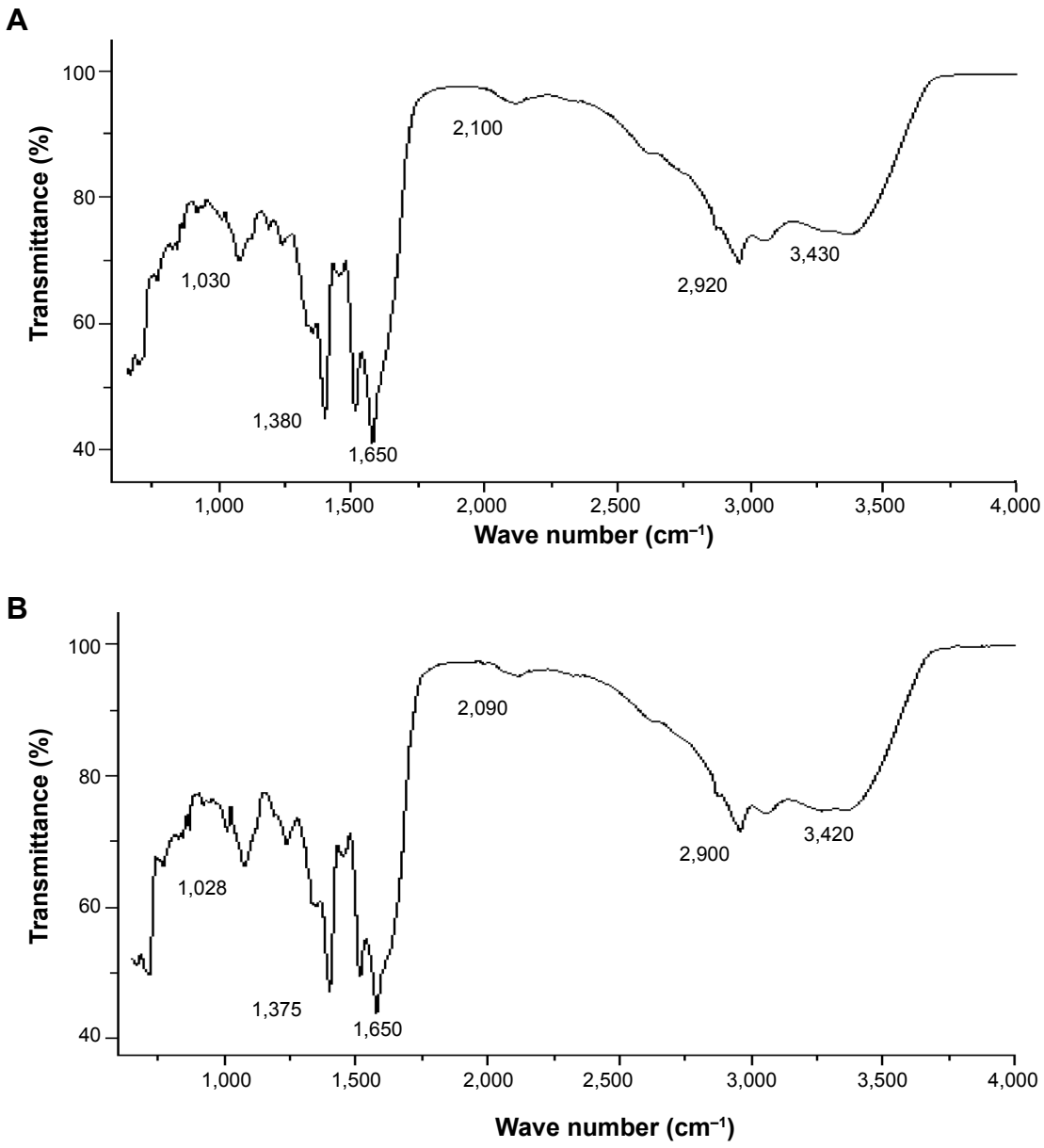

Figure 3 FTIR spectra of AgNPs with average sizes of 10 nm (**A**) and 20 nm (**B**).
Abbreviations: AgNPs, silver nanoparticles; FTIR, Fourier transform infrared spectroscopy.

random fields using TEM images that showed general morphology of AgNPs, indicating that the difference in sizes and significant difference between size distribution of different types of AgNPs (10 and 20 nm) ($P<0.05$). Figure 4A shows particles between 4 nm and 20 nm, with an average size of 10±5 nm, whereas Figure 4B shows particles between 10 nm and 50 nm, with an average size of 20±10 nm. Previous studies have reported the production of differently sized particles from various organisms such as *Klebsiella pneumoniae, B. licheniformis,* and *E. coli,* with average AgNP sizes of 52.5 nm and 50 nm.[34,38,44]

Cytotoxic effects of AgNPs in TM3 and TM4 cells

Next, cytotoxic effects of AgNPs were evaluated using in vitro models. Previous studies have reported that biologically synthesized AgNPs with an average size of 50 nm showed significant toxic effects on retinal endothelial cells.[34,45] After TM3 and TM4 cells were exposed to AgNPs for 24 hours, cell viability was assessed using the CCK-8 and MTS assays. The results of the CCK-8 assay measuring water-soluble formazan dye produced by metabolic activity of live cells showed that cell viability was decreased after exposure to

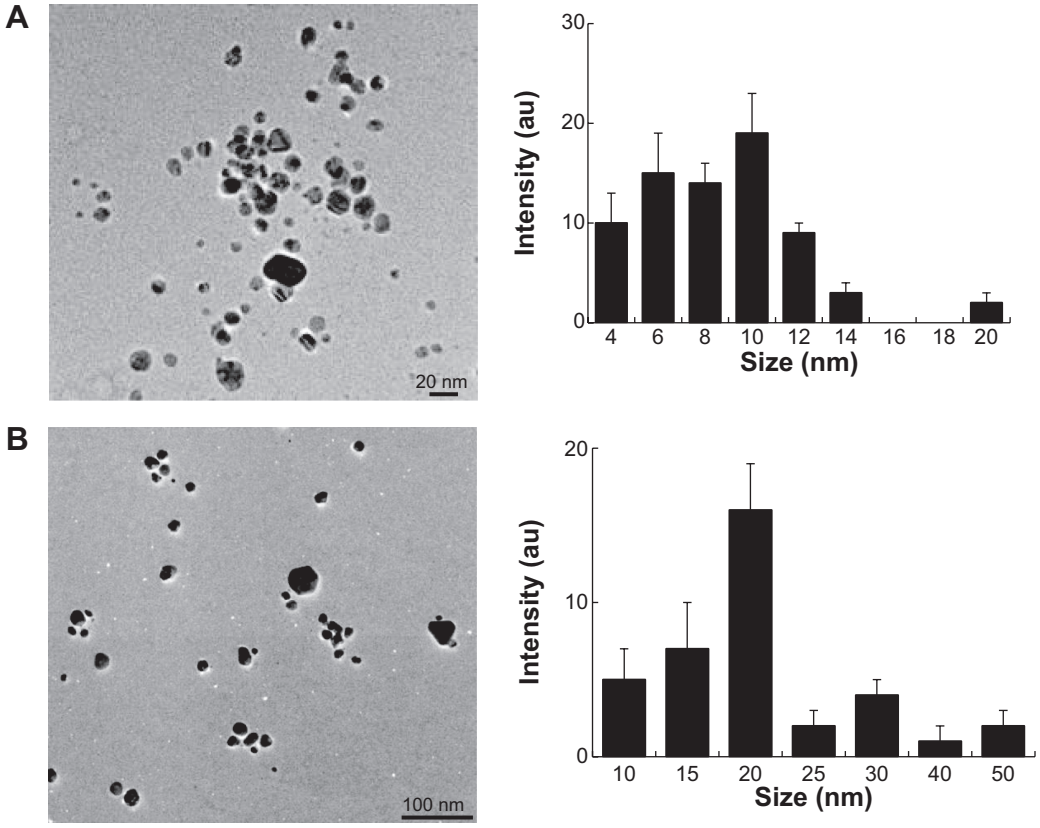

Figure 4 Transmission electron microscopy (TEM) of AgNPs.
Notes: TEM images of several fields were used to measure AgNPs particle size; micrographs (left panels) and size distributions based on TEM images (right panels) of AgNPs ranging from 4 nm to 20 nm (**A**) and 10 nm to 50 nm (**B**).
Abbreviations: AgNPs, silver nanoparticles; au, absorbance units.

AgNPs in a time- and dose-dependent manner (Figure 5A); the effects were confirmed by the MTS assay, showing that AgNPs markedly decreased cell proliferation (Figure 5B). Both assay suggested that the 10 nm nanoparticles had more significant toxicity than the 20 nm particles. Several in vitro and in vivo studies have shown that biologically synthesized AgNPs have significant cellular toxicity.[20,25,46,47] AgNPs with a size of ≤20 nm entered cells independently from endocytosis and were distributed within the cytoplasm.[48] In human glioma U251 cells, the uptake of AgNPs ≤20 nm was greater than that of AgNPs >100 nm.[49] A number of studies have reported that AgNPs are toxic to a variety of somatic cells in vitro, and can cause damage to lung, brain, and liver tissues in vivo.[15,50,51] Cytotoxicity of AgNPs in cultured cells is associated with increased generation of ROS, which have been shown to play an important role in AgNPs-induced apoptosis.[52,53] ROS are a significant factor contributing to cell death, and excessive production of ROS is known to induce apoptosis and DNA damage.[53,54] In this study, we also found that AgNPs-reduced cell viability was due to ROS generation and that accumulated ROS caused apoptosis of TM3 and TM4 cells. Our findings are consistent with those of Park et al[55] who investigated the effects of AgNPs of various sizes (20 nm, 80 nm, 113 nm) using in vitro assays for cytotoxicity, inflammation, genotoxicity, and developmental toxicity. They concluded that in all the assays, 20 nm AgNPs showed more toxicity than larger nanoparticles, which corresponds to our observations that 10 nm AgNPs were more toxic for TM3 and TM4 cells than 20 nm AgNPs, and that the IC_{50} values of 10 nm AgNPs were lower than those of 20 nm AgNPs. Further experiments were performed using the IC_{50} values of AgNPs for each cell type.

AgNPs induced production of LDH and ROS

Although apoptosis and necrosis are two morphologically different types of cell death, they are based on several common signaling mechanisms. Since various stimuli induce both apoptotic and necrotic death, the mode of cell demise seems to be dependent on intracellular factors.[56] Recent studies

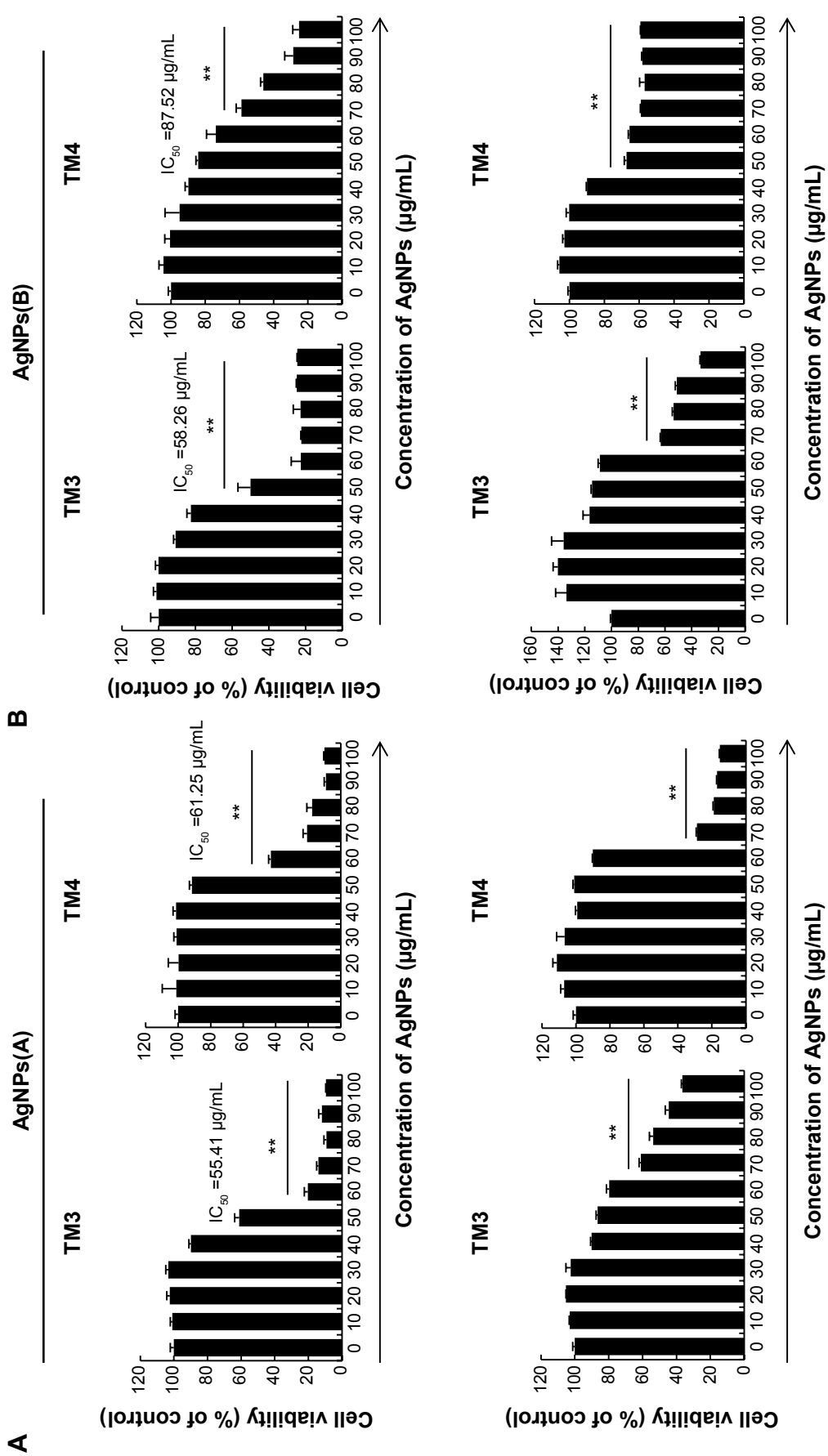

Figure 5 Effect of AgNPs on the viability of TM3 and TM4 cells.

Notes: TM3 and TM4 cells were treated with various concentrations of 10 nm (**A**) and 20 nm (**B**) AgNPs for 24 hours, and cytotoxicity was determined using the CCK-8 (top panel) and MTS (bottom panel) assays. The data are expressed as the mean ± SD of three independent experiments performed in triplicate; $^{**}p<0.01$.

Abbreviations: AgNPs, silver nanoparticles; CCK, cell counting kit-8; IC_{50}, half maximal inhibitory concentration; MTS, 3-(4,5-dimethylthiazol-2-yl)-5-(3-carboxymethoxyphenyl)-2-(4-sulfophenyl)-2H-tetrazolium, inner salt; SD, standard deviation; TM3, Leydig; TM4, Sertoli.

suggest that apoptotic and necrotic cell death involve the same receptors, signal transduction pathways, and cytotoxic mechanisms.[57–60] The LDH assay is widely used to evaluate cytotoxicity of various compounds by assessing membrane leakage, which eventually leads to cell death.

In order to determine cell membrane damage, LDH leakage into culture supernatant was measured in TM3 and TM4 cells treated with AgNPs in the presence or absence of NAC. Cell membrane integrity of TM3 and TM4 cells was compromised by AgNPs in a dose- and size-dependent manner (Figure 6A and B). To determine whether oxidative stress played a role in LDH leakage, the cells were pretreated with NAC and then LDH activity in the supernatant was analyzed. According to previous studies, the levels of reduced glutathione (GSH) are important in protecting cells from cytotoxic compounds. Antioxidants such as NAC increase intracellular GSH and decrease generation of ROS. Our results suggest that membrane leakage was ROS-dependent because in the presence of NAC, LDH release into the supernatant was reduced. Previously, Miura et al[61] have demonstrated potential cytotoxicity and increased expression levels of stress genes, *ho-1* and *mt-2A*, at higher AgNPs concentrations in HeLa cells. Kim et al[62] have reported size- and concentration-dependent cellular toxicity of AgNPs in MC3T3-E1 and PC12 cells. Collectively, these results indicate that AgNPs induced ROS production, which alter cellular redox status and stimulate LDH leakage.

ROS are considered to be general mediators of nanoparticle-induced cytotoxicity because ROS generation is a crucial component of apoptosis.[20,25,63] We assessed AgNPs-caused production of intracellular ROS using the H2DCF-DA assay, which measures peroxide-dependent oxidation of H2DCF-DA to fluorescent DCF. In TM3 and TM4 cells treated with AgNPs for 24 hours, DCF fluorescence was

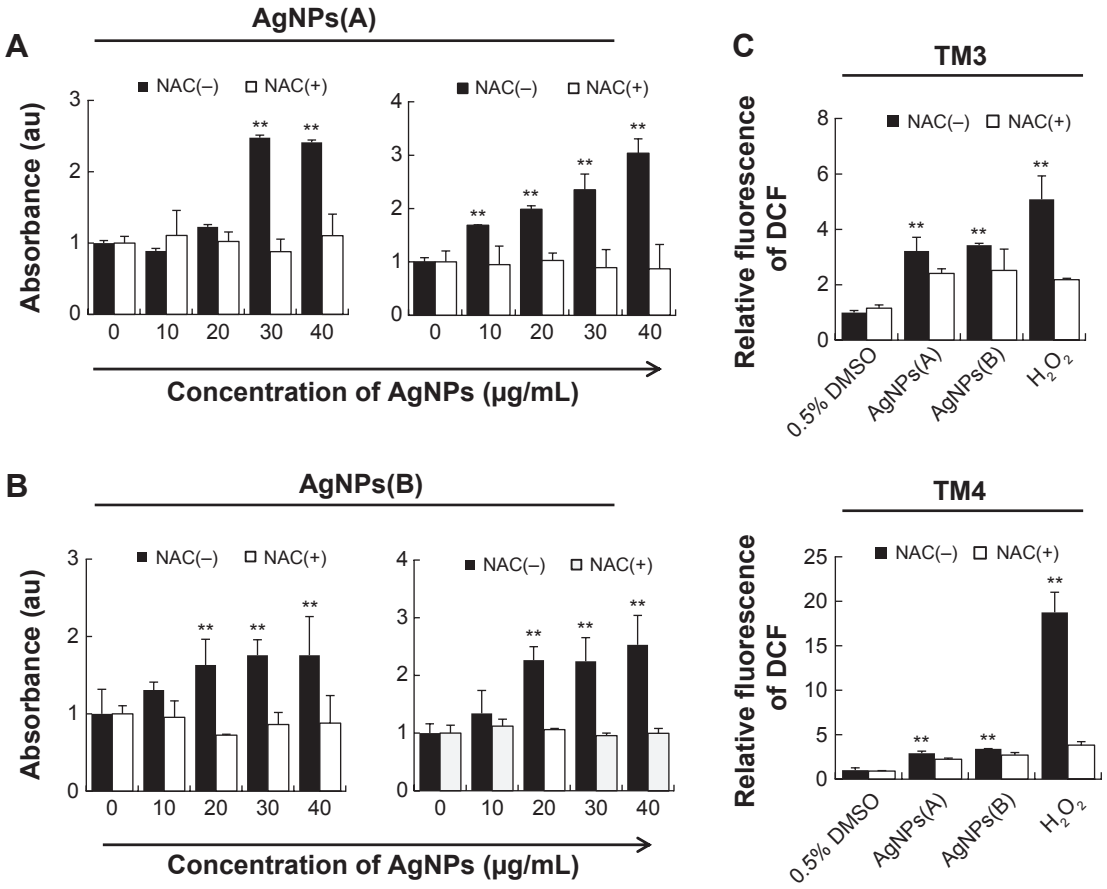

Figure 6 Effect of AgNPs on LDH activity and ROS generation in TM3 and TM4 cells.

Notes: TM3 and TM4 cells were treated with two different sizes of AgNPs: 10 nm (**A**) and 20 nm (**B**); LDH activity was assessed in the supernatants of cells treated or not with AgNPs and NAC using the LDH cytotoxicity detection kit. The y axis represents the absorbance as percentage of the controls, and the x axis shows IC_{50} of AgNPs; (**C**) ROS generation in AgNPs (IC_{50})-treated TM3 and TM4 cells; DCF formation from H2DCF-DA was measured by fluorescence (excitation at 480 nm, emission at 530 nm). The data are expressed as the mean ± SD of three independent experiments performed in triplicate; $^{**}P<0.01$.

Abbreviations: AgNPs, silver nanoparticles; DCF, 2′,7′-dichlorofluorescein; DMSO, dimethyl sulfoxide; H2DCF-DA, 2,7-dichlorodihydrofluorecein diacetate; H_2O_2, hydrogen peroxide; IC_{50}, half maximal inhibitory concentration; LDH, lactate dehydrogenase; NAC, N-acetyl L-cysteine; ROS, reactive oxygen species; SD, standard deviation; TM3, Leydig; TM4, Sertoli.

found to be markedly increased, indicating the upregulation of intracellular ROS production (Figure 6C) and suggesting that ROS are a significant factor in AgNPs cytotoxicity. To demonstrate that NAC acts as a ROS scavenger, we pretreated cells exposed to AgNPs with NAC, which significantly reduced the level of ROS generation in AgNPs-treated cells. As shown in Figure 6C, ROS generation in response to AgNPs and H_2O_2 was significantly greater than that in the control, but was alleviated by NAC; this is consistent with earlier findings, suggesting that intrinsic toxicity of AgNPs is associated with the oxidative damage-dependent pathways.[64] Thus, it appears that AgNP-induced cell death is mediated by ROS production, which may alter cellular redox status and lead to cell demise.[20,63–65]

The notion that ROS generation can be responsible for cellular damage and eventually lead to cell death in AgNPs-treated cells is in agreement with previously published results.[48,66] AgNPs generated elevated levels of intracellular ROS and reduced antioxidants such as GSH and antioxidant enzymes such as glutathione peroxidase and superoxide dismutase, resulting in the formation of DNA adducts.[20,63] Intracellular ROS have been reported to be a crucial indicator of various toxic effects exerted by nanoparticles.[67,68] Previous studies have shown that AgNPs-induced ROS generation reduces survival of different types of cells.[64,65,67–69] Rahman et al[26] have reported that 25 nm AgNPs cause a significant increase in ROS production in vitro and in vivo. Induction of apoptosis by AgNPs was mediated by oxidative stress in fibroblasts, and muscle and colon cells.[70–72] Recently, Kim et al[62] have shown that in MC3T3-E1 and PC12 cells, ROS generation is induced by AgNPs in a size- and concentration-dependent manner.

Internalization of AgNPs induced autophagosome formation

Mizushima et al[73] have reported that low-level autophagy occurs constitutively in most cells and plays an important role in cellular metabolism, growth, and development. Autophagy can be induced by endogenous physiological stress or exogenous stimuli, including chemicals and invading particles. Various types of nanomaterials have been reported to induce autophagy.[74] Cellular uptake studies have been performed to determine the effects of AgNPs on agglomeration, internalization, and formation of autophagosomes and autolysosomes and the levels of oxidative stress in these ultrastructures. TM3 and TM4 cells were exposed to AgNPs (10 nm) at the respective IC_{50} for 24 hours and then fixed and prepared for TEM analysis. Untreated cells appeared normal, with prominent nuclei, nucleoli, and mitochondria (Figure 7A–D); however, AgNPs-treated cells showed the presence of crescent shape vacuoles (Figure 7E) and multiple autophagic vacuoles consisting of double-layered membranes containing cellular debris, which were not observed in untreated cells (Figure 7F and G). AgNPs-treated cells contained several aggregates of multivesicular and membrane-rich autophagosomes, indicating that AgNPs induced autophagosome formation and alter intracellular homeostasis and adaptation to stress in TM3 and TM4 cells. In addition, AgNPs caused mitochondrial damage in TM3 and TM4 cells, not detected in the control cells (Figure 7H and J). Ultrastructural observations of TM4 cells exposed to AgNPs indicated the presence of double-membrane autophagosomes containing disintegrating material and lipid droplets (Figure 7K–M).

Yamawaki and Iwai[75] found that the treatment of human umbilical vein endothelial cells with 100 μg/mL fullerene for 24 hours resulted in its extensive internalization, vacuolization, and aggregation in autophagosomes. Similarly, Johnson-Lyles et al[76] have shown that cell death induced by fullerene exposure was linked to cytoskeleton disruption, loss of mitochondrial capacity, and autophagic vacuole accumulation. In our study, AgNPs treatment resulted in the development of double-membrane autophagosomes, autolysosomes, and autophagic vacuoles (Figure 7). Similarly, Stern et al[77] observed autophagic vacuoles in porcine kidney cells upon the treatment with cadmium selenide quantum dots; they also found that GaP quantum dots caused the development of smaller multilamellar vesicles and darkly stained lysosomal remnants. Our results are concordant with earlier reports, confirming that ultrastructural changes in TM3 and TM4 cells resulting from AgNPs treatment were consistent with lysosomal deregulation, including autophagy and autophagy-related gene expression. After 24 hours of treatment, AgNPs aggregated in the cytoplasm and appeared as dense, black inclusions in lysosomes, which are the endpoints of ingested material marked for degradation.[78] Li et al[79] have reported that gold nanoparticle-treated fibroblasts exhibit a significant number of vacuoles in the cytoplasm, many of which contained large clusters of these nanoparticles.

AgNPs induced expression of autophagy-related genes

To understand the relationship between AgNPs and autophagy, we monitored messenger RNA (mRNA) expression of *Atg6*, *Atg7*, and *Atg8* in TM3 and TM4 cells treated with the respective IC_{50} concentrations of AgNPs. Interestingly, in TM3 cells treated with AgNPs of both sizes, *Atg6* was downregulated,

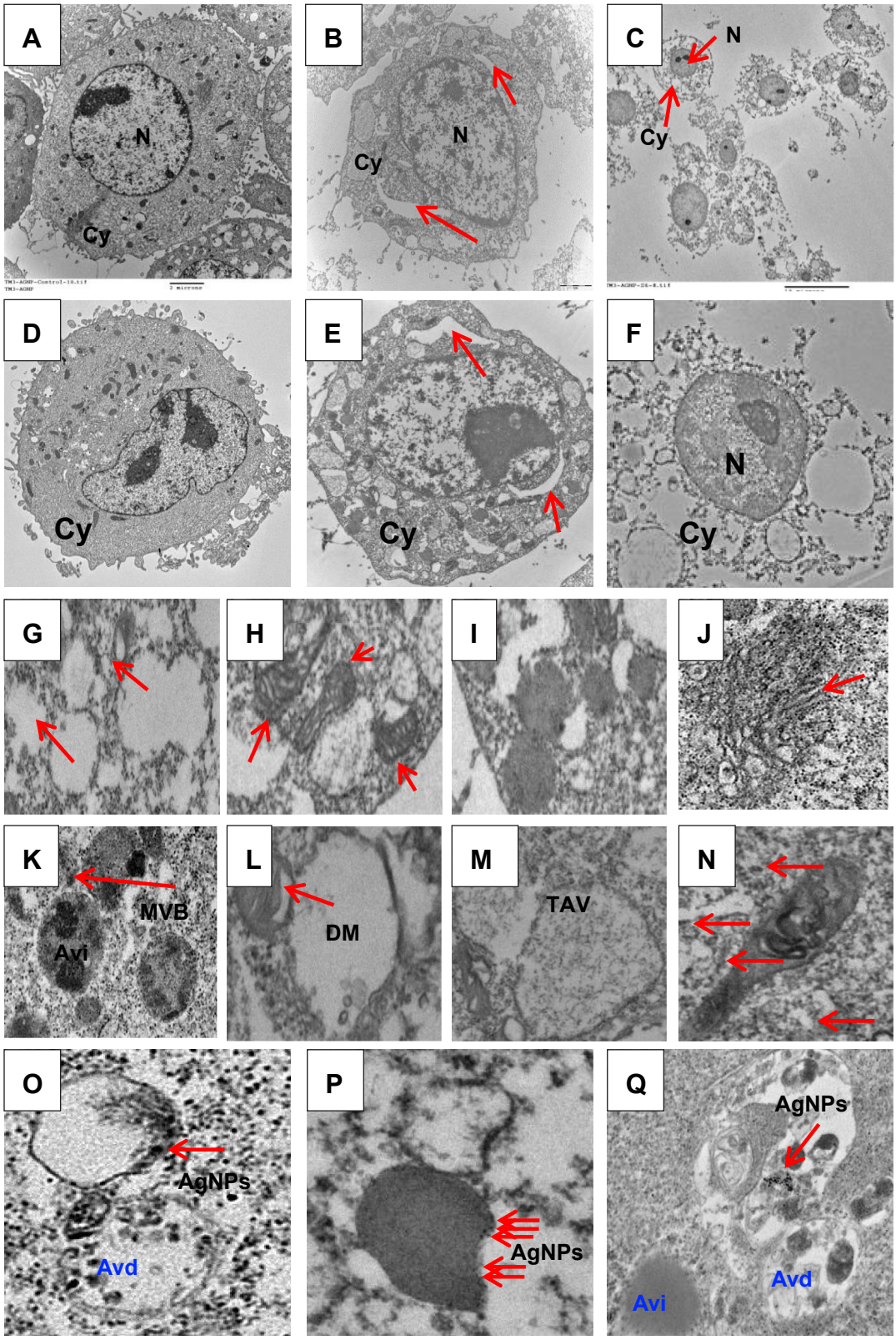

Figure 7 Cellular uptake of AgNPs induces accumulation of autophagosomes and autolysosomes.

Notes: TM3 and TM4 cells were treated with AgNPs at IC_{50} for 24 hours and analyzed by transmission electron microscopy (TEM). TEM images showed TM3 (**A**–**C**, **G**–**J**) and TM4 (**D**, **F**, **K**–**Q**) cells: not treated with AgNPs (**A**, **D**) and AgNP-treated showing crescent-like vacuoles (**B**, **E**), autophagic vacuoles (**C**, **F**), and accumulation of autophagosomes, autolysosomes, and damaged mitochondria (**G**–**J** and **K**–**Q**). Red arrows indicate the formation of autolysosomes. Autophagic vacuoles (AV) were classified into three types based on morphological criteria: AV-initial (AVi), intermediated (Avi/d), and degradative (Avd). All experiments were carried out in triplicate and repeated at least three times.

Abbreviations: AgNPs, silver nanoparticles; Cy, cytoplasm; IC_{50}, half maximal inhibitory concentration; N, nucleus; TM3, Leydig; TM4, Sertoli; TAV, typical autophagic vacuoles; DM, damaged mitochondria; MVB, multivesicular bodies.

whereas in TM4 cells, it was upregulated. Conversely, *Atg8* was significantly upregulated in TM3 cells treated with both 10 nm and 20 nm AgNPs; however, in TM4 cells, the expression of *Atg8* was not significantly affected by AgNPs. *Atg7* was significantly upregulated in both cell types (Figure 8). Interestingly, *Atg8* and *Atg6* showed opposite expression patterns in TM3 and TM4 cells, indicating the difference between TM3 and TM4 cells in the response to AgNPs. These results suggest that the regulation of autophagy-related genes depends on the nanoparticle size and cell type. Li et al[83] have observed autophagosome formation and AgNPs uptake as well as upregulation of the autophagy-related proteins microtubule-associated protein light chain 3 and autophagy gene 7 (*Atg7*) in lung fibroblast cells.

Previous studies have suggested a link between oxidative damage and autophagy.[80] The cellular role of autophagy is still not clearly understood, but it is generally thought to be a natural process involved in maintaining cellular homeostasis, as well as in the response to starvation, infection, or disease. Based on our findings and earlier studies, it can be suggested that AgNPs treatment induces oxidative stress and that the cells tried to avoid demise through induction of autophagic pathways. It is also likely that oxidative environment could trigger autophagy.[81,82] Funnell and Maysinger[83] have suggested the existence of localized sites of oxidative stress around the clusters of metal-based nanoparticles, which induce damage of the treated cells.

Effect of AgNPs on signaling molecules involved in apoptosis

Apoptosis is a part of the natural cell death processes, and is strictly controlled by interactions of multiple genes, such as those belonging to the *Bcl-2*, caspase, and *Fas* gene families as well as several oncogenes.[84,85] Fas, Bax, Bid, Bcl2, caspase-3, caspase-8, and caspase-9 are well-known proteins involved in the regulation of apoptotic cell death. It is also established that the induction of apoptosis by different cellular stresses is mediated via the MAPK cascades of JNK, Erk1/2, and p38 MAPK as well as the p53 pathway.[84–86] Therefore, we evaluated the effect of AgNPs on apoptosis and expression of apoptosis-related genes in TM3 and TM4 cells. Apoptosis was measured by flow cytometry in AgNPs-exposed cells stained with propidium iodide and Annexin V. TM3 and TM4 cells treated with AgNPs showed an increase in cellular apoptosis (Figure 9A and B), which was alleviated by the pretreatment with NAC. Previously, Foldbjerg et al[87] have demonstrated that the exposure to AgNPs results in cell cycle arrest and induction of apoptosis in human cell lines.

To evaluate the involvement of signaling molecules in AgNPs-induced apoptosis, western blot analysis was performed. Cells were treated with 10 nm and 20 nm AgNPs at respective IC_{50}, and the expression of p53, p38, p-Erk1/2, Bax, Bcl-2, RAD51, and β-actin (a reference protein) was analyzed. In TM3 cells, p53 level was upregulated more significantly by 10 nm AgNPs than by 20 nm AgNPs (Figure 9C–F), whereas p38 was not affected. Interestingly, when TM3 cells were treated with both sizes of AgNPs, the expression of Bax and RAD51 was markedly higher ($P<0.05$) than that in untreated cells, whereas Bax/Bcl-2 ratio showed no significant difference from the control. The phosphorylation of p38 and pErk1/2 in AgNPs-exposed cells was significantly higher than in the untreated cells, suggesting that AgNPs induce cytotoxicity in TM3 cells via p38- and pErk1/2-mediated pathways. In TM4 cells, p53 and p38 phosphorylation was

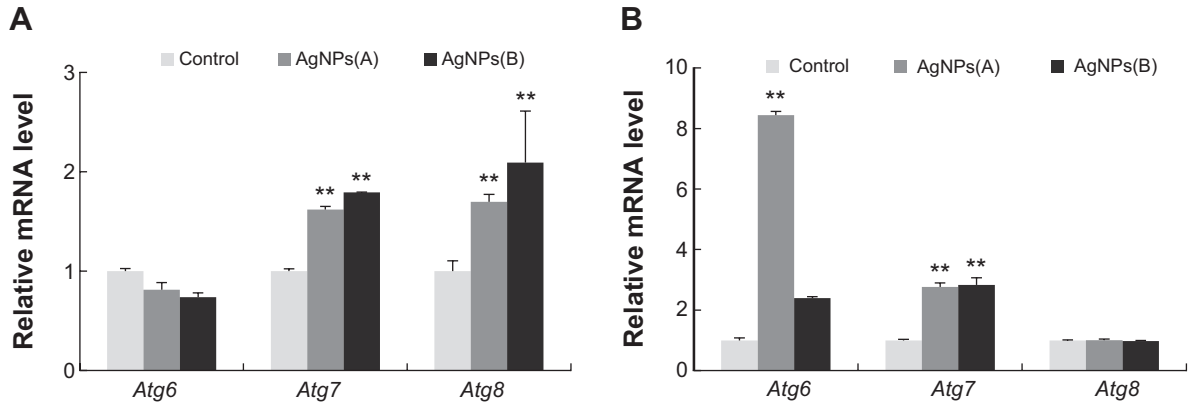

Figure 8 AgNPs accelerate expression of autophagy genes.
Notes: TM3 (**A**) and TM4 (**B**) cells were treated with AgNPs for 24 hours and analyzed for the expression of autophagy-related genes; for each treatment condition and time point, mRNA expression of AgNP-treated cells was normalized to that of untreated cells. The data are expressed as the mean relative gene expression ± SD of three independent experiments performed in triplicate; $^{**}P<0.01$.
Abbreviations: AgNPs, silver nanoparticles; mRNA, messenger RNA; SD, standard deviation; TM3, Leydig; TM4, Sertoli.

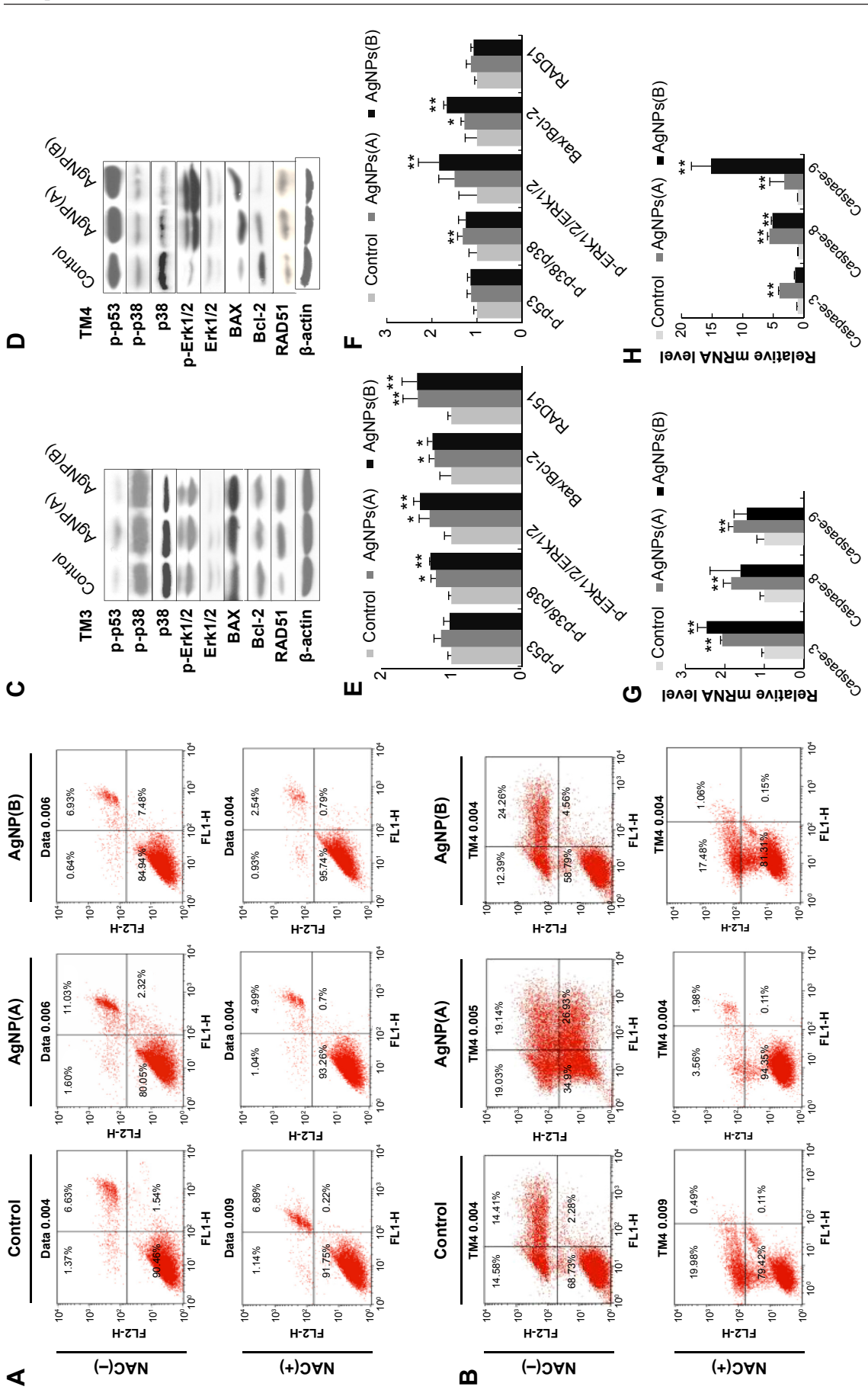

Figure 9 AgNPs promote ROS-induced apoptosis.

Notes: TM3 and TM4 cells were pretreated with 10 mM NAC for 1 hour and then treated with AgNPs for 6 hours (**A**, **B**); TM3 (**A**) and TM4 (**B**) cells were stained with Annexin V (x axis) and PI (y axis) and analyzed for cell death by flow cytometry using a FACSCanto TMII; the percentages of apoptotic cells are shown in each quadrant (**C**, **D**); TM3 (**C**) and TM4 (**D**) cells were exposed to the respective IC_{50} of AgNPs for 6 hours and analyzed for protein expression by western blotting using the indicated antibodies; (**E**, **F**) protein expression relative to β-actin used as the loading control; (**G**, **H**) relative mRNA expression levels of apoptotic genes analyzed by RT-PCR. The data are expressed as the mean relative gene expression ± SD of three independent experiments performed in triplicate; *$P<0.05$, **$P<0.01$.

Abbreviations: AgNPs, silver nanoparticles; IC_{50}, half maximal inhibitory concentration; mRNA, messenger RNA; NAC, N-acetyl L-cysteine; PI, propidium iodide; ROS, reactive oxygen species; RT-PCR, real-time polymerase chain reaction; SD, standard deviation; TM3, Leydig; TM4, Sertoli.

not significantly affected, whereas the phosphorylation of Erk1/2, Bax, Bcl2, and RAD51 increased (Figure 9D–F, $P<0.05$). The results of the western blot experiments suggest that AgNPs induce two different signaling pathways in TM3 and TM4 cells, depending on AgNPs size and cell type.

Mitochondria play an important role in apoptosis via the intrinsic apoptotic program, which includes caspase activation. Therefore, we examined the effects of AgNPs on caspase-3, caspase-8, and caspase-9 using quantitative RT-PCR. The results showed that mRNA expression of these caspases was significantly higher in AgNPs-treated than in the control TM3 and TM4 cells (Figure 9G and H). Apoptosis signal transduction includes a cascade of initiator and executioner caspases.[88] Initiator caspases 8 and 9 activate executioner caspases 3 and 7, which then cleave specific substrates, leading to apoptosis and ultimately cell death.[89] In our studies, AgNPs significantly upregulated the expression of caspases 3, 8, and 9 (Figure 9G and H). Mitochondrial permeability has been associated with various metabolic consequences, such as halted electron transport, generation of ROS, and decreased production of ATP.[90,91] Collectively, our results suggest that AgNPs of both sizes upregulate caspase mRNA; however, 10 nm particles produced a significantly stronger effect than the 20 nm particles, and TM3 cells were more sensitive than TM4 cells.

Rapid generation of ROS could directly activate both intrinsic and extrinsic apoptotic pathways. The activation of MAPKs plays an essential role in apoptosis induced by cellular stresses.[92] We found that AgNP treatment resulted in the activation of MAPK/Erk signaling (Figure 9C), suggesting that the Erk1/2 pathway mediates AgNPs-induced cellular cytotoxicity. Because of the essential role of Bcl-2 and Bax in the regulation of apoptosis, we examined the effects of AgNPs on the expression of these proteins.[84,93] As shown in Figure 9, in TM3 and TM4 cells, AgNPs decreased expression of the antiapoptotic protein Bcl-2 and increased that of the proapoptotic protein Bax, which increased the Bax/Bcl2 ratio. As shown in Figure 9, AgNPs regulated apoptosis via the p38-MAPK signal transduction pathway in TM3 cells. ROS play an important role in apoptosis through induction of DNA damage,[94,95] which increases p53 expression, triggering cell cycle arrest to provide the time for DNA repair. AgNPs activated the expression of the cell cycle checkpoint protein p53 and the DNA damage repair protein Rad51 in the treated cells (Figure 9), suggesting p53-mediated apoptosis.[96,97] Taken together, these data indicate that AgNPs induce apoptosis of TM3 and TM4 cells through activation of the p53 and MAPK pathways.

AgNPs effect on the expression of genes encoding steroidogenic and tight junction proteins

We examined whether AgNPs have an effect on the expression of genes involved in steroidogenesis in TM3 cells and encoding tight junction proteins in TM4 cells. The cells were treated with AgNPs at IC_{50} and mRNA levels of cytochrome P450 side-chain cleavage (*P450scc*), steroidogenic acute regulatory protein (StAR), 3β-hydroxysteroid dehydrogenase (*3β-Hsd*), 17-hydroxysteroid dehydrogenase (*17β-Hsd*), luteinizing hormone receptor (*LhR*), and cytochrome P450 17A1 (*Cyp17a1*) were determined by RT-PCR. As shown in Figure 10A, the expression of *StAR, 3β-Hsd, 17β-Hsd,* and *Cyp17a1* mRNA was significantly downregulated, whereas that of *LhR* and *Cyp19a1* mRNA was not altered. This observation indicates that AgNPs could inhibit the synthesis of male steroid hormones and cause apoptosis of male germ cells during spermatogenesis. Testosterone secreted by Leydig cells is necessary for completion of spermatogenesis and maintenance of secondary sexual characteristics. Previous studies have demonstrated that testosterone biosynthesis depends on the expression of steroidogenic genes, including *P450scc*, *StAR*, *3β-HSD*, and *Cyp17a1*.[98,99]

Leydig cells, the primary producers of steroid hormones, play a major role in the male reproductive system by releasing testosterone.[100] Testosterone synthesis occurs through a series of enzymatic reactions involving members of the cytochrome P450 family (Cyp11a1 and Cyp17a1), and hydroxysteroid dehydrogenases 3β-HSD and 17β-HSD. StAR mediates cholesterol transfer from the outer to inner mitochondrial membrane, which is a rate-limiting step in steroid biosynthesis,[101,102] and suppression of *StAR* transcription and/or translation leads to a significant reduction in steroidogenesis.[103,104] Exposure to specific chemicals has been shown to affect testosterone production in Leydig cells by interfering with the expression of *Cyp17a1, P450scc*, and *StAR*.[19,105] We observed a significant decrease in *StAR*, *3β-HSD*, *17β-HSD*, and *Cyp17a1* mRNA levels in AgNPs-treated TM3 cells (Figure 10A). *P450scc* encodes a cholesterol side-chain cleavage enzyme considered to be a rate-limiting step in the synthesis of testosterone.[98,99] However, mRNA levels of P450 enzymes were not significantly different between the control and AgNPs-treated cells (Figure 10A). Decreased expression of *Cyp17a1* and *17β-HSD* may be partially due to the reduced levels of *StAR* and *3β-HSD*, and can result in a decrease of testosterone production.[105] Collectively, these

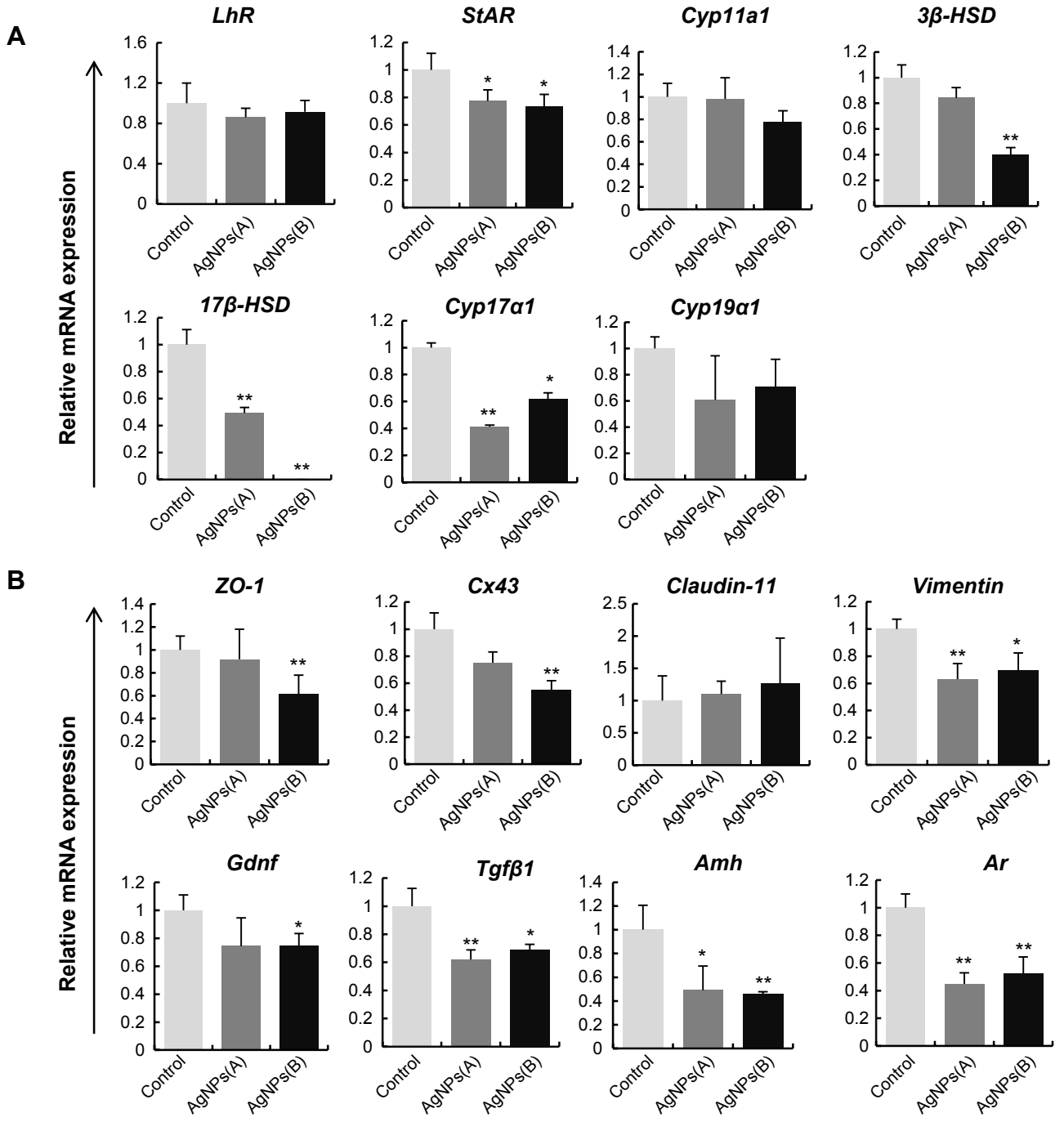

Figure 10 Effect of AgNPs on gene expression in TM3 and TM4 cells.

Notes: (**A**) Quantitative (q) RT-PCR for testosterone biosynthesis-related genes in TM3 cells; (**B**) qRT-PCR for the BTB genes *Gdnf*, *Tgfβ1*, *Ar*, and *Amh* in TM4 cells. The expression of all genes was normalized to that of *Gapdh*. The data are expressed as the mean relative gene expression ± SD of three independent experiments performed in triplicate; *$P<0.05$, **$P<0.01$.

Abbreviations: AgNPs, silver nanoparticles; BTB, blood–testes barrier; mRNA, messenger RNA; RT-PCR, real-time polymerase chain reaction; SD, standard deviation; TM3, Leydig; TM4, Sertoli; qRT-PCR, quantitative RT-PCR.

results indicate that the exposure to AgNPs inhibits *StAR, 3β-HSD*, and *17β-HSD* transcription, which can negatively affect testosterone production in TM3 cells. Sertoli cells are the main somatic cells in the testes, which play a key role in spermatogenesis by providing structural support, synthesizing and releasing specific proteins to regulate responses to pituitary hormone release, and presenting immune barrier for germ cells.[106]

We next examined the expression of tight junction genes in AgNPs-treated TM4 (Sertoli) cells. The *ZO-1*, *Cx43*,

Cldn11, and *Vim* genes encode tight junction proteins, which play a key role in the formation of the blood–testes barrier (BTB). In TM4 cells, AgNPs reduced mRNA levels of *ZO-1* and *Cx43*, whereas those of *Cldn11* were not significantly altered (Figure 10B). These findings imply that AgNPs may influence the expression of tight junction proteins, which play key roles in the maintenance of BTB functions. Tight junction proteins ZO-1, Claudin-11, and connexin-43 are important structural components of Sertoli cells essential to BTB function.[107–109] Deregulation of these genes is observed in a number of diseases. Environmental toxins can impair the viability and function of Sertoli cells, inducing BTB disruption.[109–111] Our findings demonstrate that *ZO-1* and *Cx43* were targeted by AgNPs, as evidenced by the decreased level of their mRNA in TM4 cells exposed to AgNPs, whereas *Ocln-11* did not show significant changes (Figure 10B). Vimentin expression is considered an indicator of the early effects of testicular toxins. As shown in Figure 10B, *Vim* expression was downregulated in TM4 cells after the exposure to AgNPs, suggesting that AgNPs could affect the development of germ cells in the testes. Overall, the harmfulness of nanoparticles may closely correlate with their size-related ability to readily enter biological systems. However, size is not the only factor that governs toxicity; other factors such as concentration of nanoparticles, surface charge, and type of cells also play important roles.

We also examined the expression of the genes encoding specific secretory proteins, *Amh*, *Gdnf*, and *Tgfβ1* in TM4 cells using RT-PCR. These secretory proteins play important roles in self-renewal, proliferation, and differentiation of SSCs. The mRNA levels of *Gdnf*, *Tgfβ1*, *Ar*, and *Amh* genes were significantly lower in AgNPs-treated cells than in the control group (Figure 10B), further confirming that AgNPs were cytotoxic for Sertoli cells. GDNF, secreted by these cells, is essential for self-renewal, proliferation, and differentiation of SSCs.[107,108] The cells exposed to AgNPs showed reduced *Gdnf* mRNA expression, indicating that AgNPs exposure may downregulate GDNF synthesis and secretion (Figure 10B). Overall, these results suggest that AgNPs exposure could affect the development of germ cells in the testes, and ultimately cause reproductive toxicity.

Characterization of SSCs

Leydig, Sertoli, and SSCs are key players working in concert in the regulation of spermatogenesis. Testosterone secreted by Leydig cells is necessary for both spermatogenesis and function of Sertoli cells, which secrete proteins necessary for SSC proliferation and self-renewal. SSCs continuously produce male gametes throughout postnatal life.[112] To determine the effects of AgNPs on the entire process of spermatogenesis, we isolated and characterized SSCs from mouse testes. Stem cells in the male germ line undergo dramatic functional and morphological transformations necessary for spermatogenesis, and it is important to identify the SSC unique molecular and functional characteristics. RT-PCR was performed to assess the expression of multipotent marker genes such as *Oct4*, *Rex-1*, and *Sycp3*, commonly expressed in SSCs and embryonic stem cells; *Nanog*, a specific marker for ESCs; and *Tex-18*, *Zbtb16*, and *Vasa*, expressed only in SSCs (*Gapdh* served as an internal control). RT-PCR analysis shows that all selected markers except *Nanog* demonstrated strong expression in SSCs (Figure 11A). Protein levels of SSC transcription factor Oct4 and cytoplasmic SSC markers vasa, Ep-CAM, and CD49f were evaluated by immunostaining (Figure 11B). Ryu et al[112] observed a similar pattern in SSCs from rat testes. Furthermore, the expression of vasa, thymocyte antigen 1.2, and integrin α-6/β-1 in SSCs was analyzed by FACS (Figure 11C), which indicated that a significant number of cells in SSC clumps were positive for the targeted proteins. FACS analysis also demonstrated an enriched SSC population, as evidenced by the expression of Thy-1 (CD90), a glycoprotein in the immunoglobulin superfamily expressed in a variety of stem cells, including mouse SSCs.[112–114]

Effects of AgNPs-treated TM3 and TM4 on SSCs

SSCs were cultured for 72 hours with AgNPs-treated TM3 or TM4 as feeder cells, and then subjected to FACS analysis to determine the percentage of SSCs and relative mRNA expression of the genes involved in SSC meiosis, differentiation, and self-renewal. The percentage of SSCs was not significantly different in the treated and untreated groups (Figure 12A and B). RT-PCR analysis revealed that the mRNA levels of the meiosis genes *Stra8*, *Dazl*, and *Sycp3* and the differentiation marker gene *c-Kit* were significantly lower in AgNPs-treated cells than in control, whereas the gene encoding self-renewal marker proliferating cell nuclear antigen (PCNA) was not significantly affected, which may be due to the lack of PCNA involvement in repair mechanisms such as base excision repair, nucleotide excision repair, and mismatch repair in TM3 and TM4 cells. Interestingly, the expression of genes downstream of *Gdnf*, such as *Bcl-6* and *Etv5*, was significantly reduced in SSCs (Figure 12C).

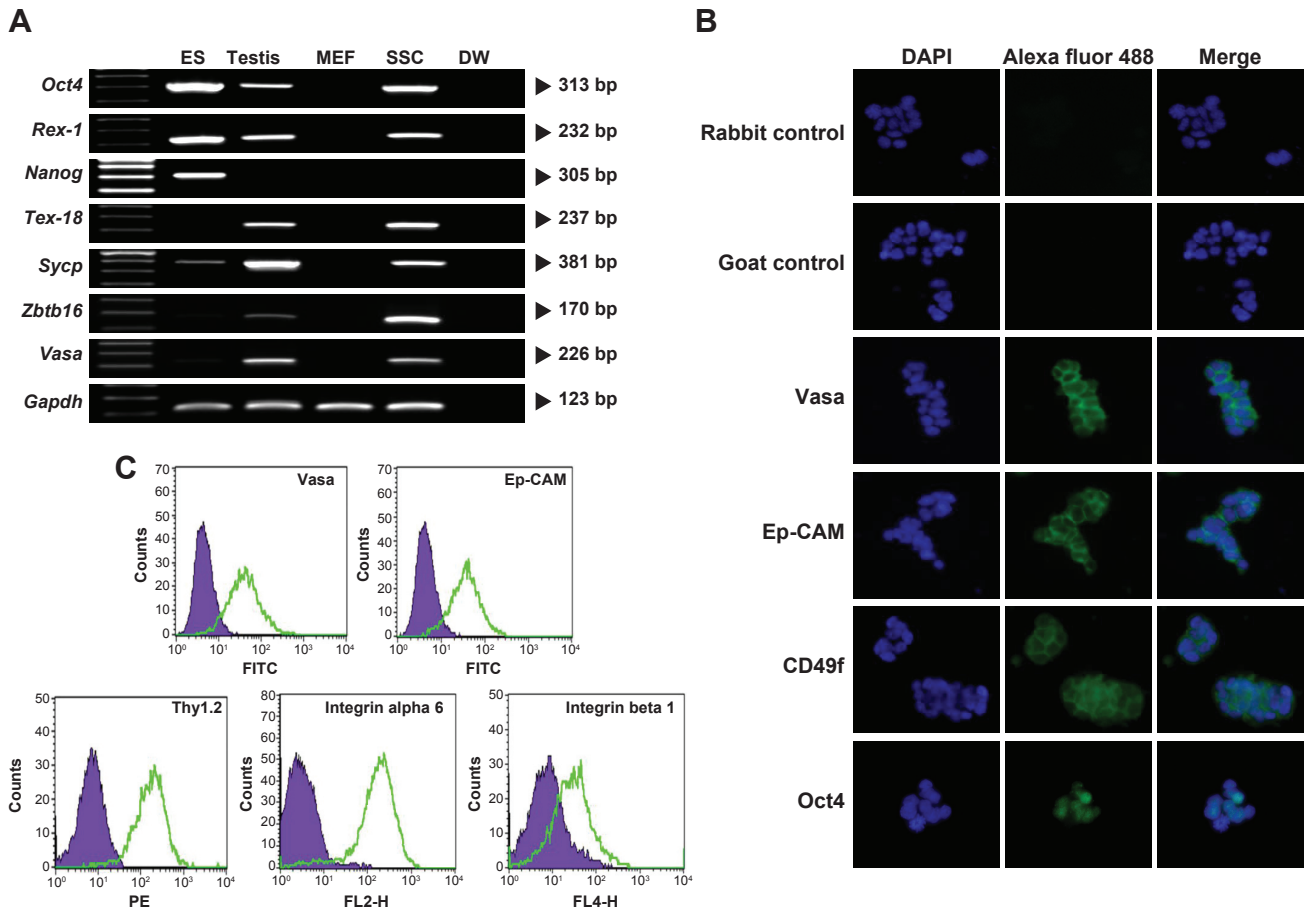

Figure 11 Characterization of SSCs using RT-PCR, immunostaining, and FACS.
Notes: (**A**) RT-PCR was performed to assess the expression of multipotent marker genes *Oct3/4*, *Rex-1*, *Nanog*, *Tex-18*, *Sycp3*, *Zbtb16*, and *Vasa*; (**B**) immunostaining analysis confirmed the expression of Oct4, vasa, Ep-CAM, and CD49f; (**C**) FACS analysis of the expression of vasa, Thy1.2, integrin α-6, and integrin β-1 in SSCs.
Abbreviations: DAPI, 4′,6-diamidino-2-phenylindole, dihydrochloride; DW, distilled water; ES, embryonic stem cells; FACS, fluorescence-activated cell sorting; MEF, mouse embryonic fibroblasts; RT-PCR, real-time polymerase chain reaction; SSCs, spermatogonial stem cells; FITC, fluorescein isothiocyanate.

Earlier studies have suggested that GDNF is essential for SSC self-renewal and proliferation, stimulating the growth of C18-4 cells.[71,115] Braydich-Stolle et al[71] have reported that cells cultured with 10 µg/mL of AgNPs decreased proliferation of SSCs.

SSCs are the progenitors of male germ cells, while Leydig and Sertoli cells are the somatic cells in the testes important for proliferation, self-renewal, and differentiation of SSCs.[116] The main function of Leydig cells in the testes is the synthesis and secretion of testosterone, important for germ cell production from SSCs, ie, spermatogenesis. Sertoli cells provide physical support for SSCs and also express proteins and other factors, such as GDNF, SCF, and BMP4, which regulate all aspects of germ cell development.[115–117] Proliferation and differentiation of SSCs is particularly sensitive to environmental insults such as chemicals and physical stressors.[117] Any chemical compound that affects the viability and function of Leydig and Sertoli cells may affect spermatogenesis. Braydich-Stolle et al[71] have revealed that 10 µg/mL of AgNPs inhibited SSC proliferation in vitro. Zhang et al[108] have shown that lipopolysaccharide inhibits the expression of GDNF in Sertoli cells and prevents SSC self-renewal via downregulation of GDNF-targeted genes. Collectively, our results suggest that AgNPs have a significant negative impact on spermatogenesis and expression of tight junction proteins involved in the regulation of germ cell cycle progression, cell proliferation, and cell motility. The treatment of Leydig, Sertoli, and SSCs with AgNPs impaired the functions of these cells, which are critically important for spermatogenesis. This study further confirms that AgNPs could cause reproductive toxicity in male somatic cells and SSCs.

Acknowledgment

This work was supported by the KU-Research Professor Program of Konkuk University. Dr Sangiliyandi Gurunathan

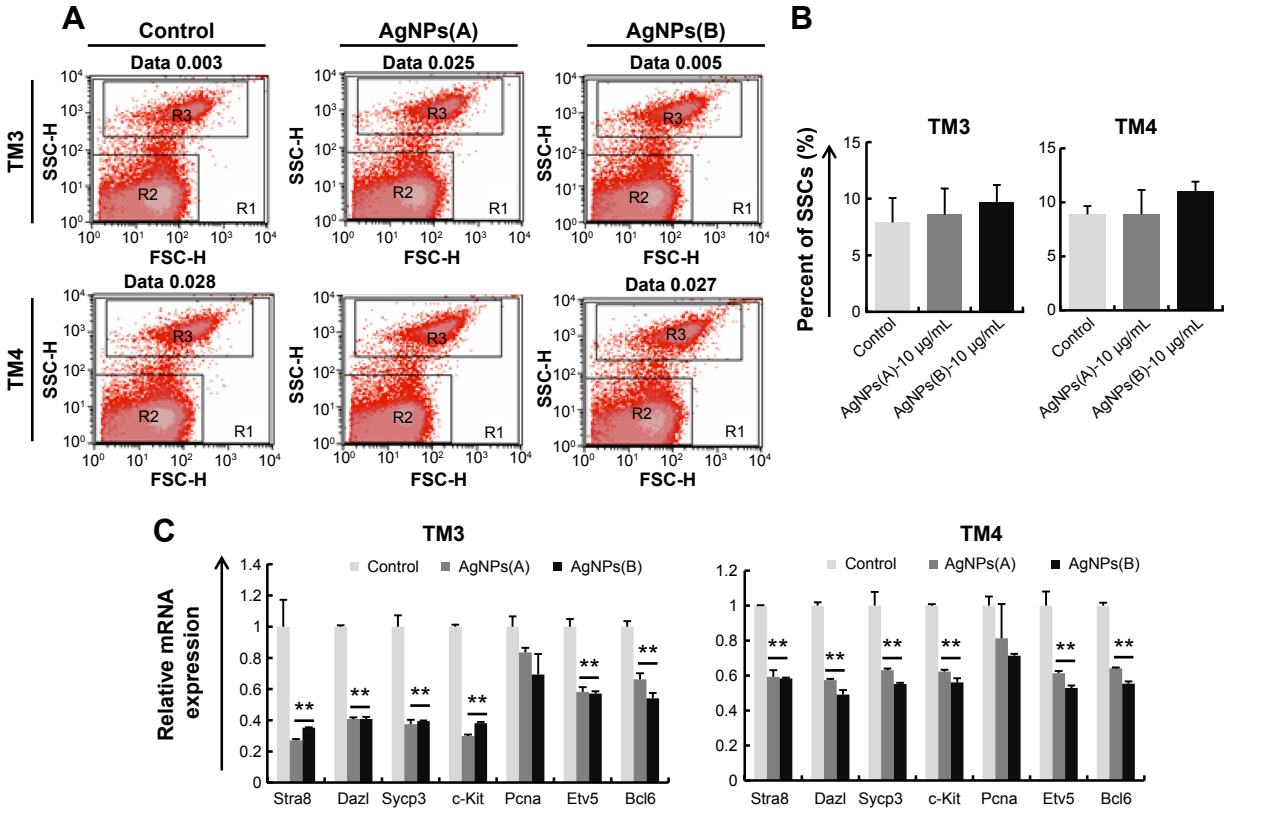

Figure 12 Effects of AgNPs on the proliferation and differentiation of SSCs.

Notes: (**A**) FACS analysis of SSCs using CD49f antibody; (**B**) the percentage of SSCs cultured on TM3 or TM4 as feeder cells; (**C**) expression of the genes involved in meiosis, self-renewal, and differentiation assessed by quantitative RT-PCR and normalized to that of Gapdh. Incubation of SSCs on TM3 and TM4 cells treated with AgNP (10 μg/mL) caused a significant decrease in mRNA levels of the analyzed genes. The results are presented as mean ± SEM of triplicate measurements; $^{**}P<0.01$.

Abbreviations: AgNPs, silver nanoparticles; FACS, fluorescence-activated cell sorting; RT-PCR, real-time polymerase chain reaction; SEM, standard error of the mean; SSCs, spermatogonial stem cells; TM3, Leydig; TM4, Sertoli; FSC-H, forward scatter-height.

was supported by the Konkuk University KU-Full-time Professorship. This work was also supported by the Woo Jang-Choon Project (PJ007849).

Disclosure

The authors report no conflicts of interest in this work.

References

1. Morrow KJ, Bawa R, Wei C. Recent advances in basic and clinical nanomedicine. *Med Clin North Am*. 2007;91(5):805–843.
2. Jain J, Arora S, Rajwade JM, Omray P, Khandelwal S, Paknikar KM. Silver nanoparticles in therapeutics: development of an antimicrobial gel formulation for topical use. *Mol Pharm*. 2009;6(5):1388–1401.
3. Park EJ, Yi J, Kim Y, Choi K, Park K. Silver nanoparticles induce cytotoxicity by a Trojan-horse type mechanism. *Toxicol In Vitro*. 2010;24(3):872–878.
4. Chen X, Schluesener HJ. Nanosilver: a nanoproduct in medical application. *Toxicol Lett*. 2008;176(1):1–12.
5. Awazu K, Fujimaki M, Rockstuhl C, et al. A plasmonic photocatalyst consisting of silver nanoparticles embedded in titanium dioxide. *J Am Chem Soc*. 2008;130(5):1676–1680.
6. Velmurugan P, Iydroose M, Mohideen MH, Mohan TS, Cho M, Oh BT. Biosynthesis of silver nanoparticles using Bacillus subtilis EWP-46 cell-free extract and evaluation of its antibacterial activity. *Bioprocess Biosyst Eng*. 2014;37(8):1527–1534.
7. Sondi I, Salopek-Sondi B. Silver nanoparticles as antimicrobial agent: a case study on E. coli as a model for Gram-negative bacteria. *J Colloid Interface Sci*. 2004;275:177–182.
8. Elechiguerra JL, Burt JL, Morones JR, et al. Interaction of silver nanoparticles with HIV-1. *J Nanobiotechnology*. 2005;3:6.
9. Dobrovolskaia MA, McNeil SE. Immunological properties of engineered nanomaterials. *Nat Nanotechnol*. 2007;2(8):469–478.
10. Hussain N, Jaitley V, Florence AT. Recent advances in the understanding of uptake of microparticulates across the gastrointestinal lymphatics. *Adv Drug Deliv Rev*. 2001;50(1–2):107–142.
11. Jeong GN, Jo UB, Ryu HY, Kim YS, Song KS, Yu IJ. Histochemical study of intestinal mucins after administration of silver nanoparticles in Sprague-Dawley rats. *Arch Toxicol*. 2010;84(1):63–69.
12. Kim YS, Kim JS, Cho HS, et al. Twenty-eight-day oral toxicity, genotoxicity, and gender-related tissue distribution of silver nanoparticles in Sprague-Dawley rats. *Inhal Toxicol*. 2008;20(6):575–583.
13. Kim YS, Song MY, Park JD, et al. Subchronic oral toxicity of silver nanoparticles. *Part Fibre Toxicol*. 2010;7:20.
14. Cha K, Hong HW, Choi YG, et al. Comparison of acute responses of mice livers to short-term exposure to nano-sized or micro-sized silver particles. *Biotechnol Lett*. 2008;30(11):1893–1899.
15. Sung JH, Ji JH, Yoon JU, et al. Lung function changes in Sprague-Dawley rats after prolonged inhalation exposure to silver nanoparticles. *Inhal Toxicol*. 2008;20(6):567–574.
16. Jang MH, Kim WK, Lee SK, Henry TB, Park JW. Uptake, tissue distribution, and depuration of total silver in common carp (Cyprinus carpio) after aqueous exposure to silver nanoparticles. *Environ Sci Technol*. 2014;48(19):11568–11574.
17. Park EJ, Bae E, Yi J, et al. Repeated-dose toxicity and inflammatory responses in mice by oral administration of silver nanoparticles. *Environ Toxicol Pharmacol*. 2010;30(2):162–168.

18. Lee Y, Kim P, Yoon J, et al. Serum kinetics, distribution and excretion of silver in rabbits following 28 days after a single intravenous injection of silver nanoparticles. *Nanotoxicology*. 2013;7(6):1120–1130.
19. Garcia TX, Costa GM, França LR, Hofmann MC. Sub-acute intravenous administration of silver nanoparticles in male mice alters Leydig cell function and testosterone levels. *Reprod Toxicol*. 2014;45:59–70.
20. AshaRani PV, Low Kah Mun G, Hande MP, Valiyaveettil S. Cytotoxicity and genotoxicity of silver nanoparticles in human cells. *ACS Nano*. 2009; 3(2):279–290.
21. Avalos A, Haza AI, Mateo D, Morales P. Interactions of manufactured silver nanoparticles of different sizes with normal human dermal fibroblasts. *Int Wound J*. Epub 2014 Feb 25.
22. Gliga AR, Skoglund S, Wallinder IO, Fadeel B, Karlsson HL. Size-dependent cytotoxicity of silver nanoparticles in human lung cells: the role of cellular uptake, agglomeration and Ag release. *Part Fibre Toxicol*. 2014;11:11.
23. Samberg ME, Loboa EG, Oldenburg SJ, Monteiro-Riviere NA. Silver nanoparticles do not influence stem cell differentiation but cause minimal toxicity. *Nanomedicine (Lond)*. 2012;7(8): 1197–1209.
24. Mei N, Zhang Y, Chen Y, et al. Silver nanoparticle-induced mutations and oxidative stress in mouse lymphoma cells. *Environ Mol Mutagen*. 2012;53(6):409–419.
25. Gurunathan S, Han JW, Eppakayala V, Jeyaraj M, Kim JH. Cytotoxicity of biologically synthesized silver nanoparticles in MDA-MB-231 human breast cancer cells. *Biomed Res Int*. 2013;2013: 535796.
26. Rahman MF, Wang J, Patterson TA, et al. Expression of genes related to oxidative stress in the mouse brain after exposure to silver-25 nanoparticles. *Toxicol Lett*. 2009;187(1):15–21.
27. Wang J, Wang WX. Salinity influences on the uptake of silver nanoparticles and silver nitrate by marine medaka (Oryzias melastigma). *Environ Toxicol Chem*. 2014;33(3):632–640.
28. Christen V, Capelle M, Fent K. Silver nanoparticles induce endoplasmatic reticulum stress response in zebrafish. *Toxicol Appl Pharmacol*. 2013; 272(2):519–528.
29. Zhang Z, Zhang X, Sun Z, et al. Cytochrome P450 3A1 mediates 2,2′,4,4′-tetrabromodiphenyl ether-induced reduction of spermatogenesis in adult rats. *PLoS One*. 2013;8(6):e66301.
30. Bellot GL, Liu D, Pervaiz S. ROS, autophagy, mitochondria and cancer: Ras, the hidden master? *Mitochondrion*. 2013;13(3):155–162.
31. Esposito LA, Melov S, Panov A, Cottrell BA, Wallace DC. Mitochondrial disease in mouse results in increased oxidative stress. *Proc Natl Acad Sci U S A*. 1999;96(9):4820–4825.
32. Ito K, Hirao A, Arai F, et al. Reactive oxygen species act through p38 MAPK to limit the lifespan of hematopoietic stem cells. *Nat Med*. 2006; 12(4):446–451.
33. Choi YJ, Kim NH, Lim MS, Lee HJ, Kim SS, Chun W. Geldanamycin attenuates 3-nitropropionic acid-induced apoptosis and JNK activation through the expression of HSP 70 in striatal cells. *Int J Mol Med*. 2014; 34(1):24–34.
34. Gurunathan S, Kalishwaralal K, Vaidyanathan R, et al. Biosynthesis, purification and characterization of silver nanoparticles using Escherichia coli. *Colloids Surf B Biointerfaces*. 2009;74(1):328–335.
35. Han JW, Gurunathan S, Jeong JK, et al. Oxidative stress mediated cytotoxicity of biologically synthesized silver nanoparticles in human lung epithelial adenocarcinoma cell line. *Nanoscale Res Lett*. 2014;9(1):459.
36. Sastry CS, Srinivas Y, Rao PV. Assay of cisapride in pharmaceutical formulations by extraction spectrophotometry. *Talanta*. 1997;44(4):517–526.
37. Jain D, Kachhwaha S, Jain R, Srivastava G, Kothari SL. Novel microbial route to synthesize silver nanoparticles using spore crystal mixture of Bacillus thuringiensis. *Indian J Exp Biol*. 2010;48(11):1152–1156.
38. Kalimuthu K, Suresh Babu R, Venkataraman D, Bilal M, Gurunathan S. Biosynthesis of silver nanocrystals by Bacillus licheniformis. *Colloids Surf B Biointerfaces*. 2008;65(1):150–153.
39. Khalil MMH, Ismail EH, El-Baghdady KZ, Mohamed D. Green synthesis of silver nanoparticles using olive leaf extract and its antibacterial activity. *Arabian J Chemis*. 2014;7(6):1131–1139.
40. Pasupuleti VR, Prasad, Shiekh RA, et al. Biogenic silver nanoparticles using Rhinacanthus nasutus leaf extract: synthesis, spectral analysis, and antimicrobial studies. *Int J Nanomedicine*. 2013;8:3355–3364.
41. Gurunathan S, Han JW, Kwon DN, Kim JH. Enhanced antibacterial and anti-biofilm activities of silver nanoparticles against Gram-negative and Gram-positive bacteria. *Nanoscale Res Lett*. 2014;9(1):373.
42. Gole A, Dash C, Soman C, Sainkar SR, Rao M, Sastry M. On the preparation, characterization, and enzymatic activity of fungal protease-gold colloid bioconjugates. *Bioconjug Chem*. 2001;12(5):684–690.
43. Vigneshwaran N, Kathe AA, Varadarajan PV, Nachane RP, Balasubramanya RH. Silver-protein (core-shell) nanoparticle production using spent mushroom substrate. *Langmuir*. 2007;23(13):7113–7117.
44. Shahverdi AR, Fakhimi A, Shahverdi HR, Minaian S. Synthesis and effect of silver nanoparticles on the antibacterial activity of different antibiotics against Staphylococcus aureus and Escherichia coli. *Nanomedicine*. 2007;3(2):168–171.
45. Kalishwaralal K, Banumathi E, Ram Kumar Pandian S, et al. Silver nanoparticles inhibit VEGF induced cell proliferation and migration in bovine retinal endothelial cells. *Colloids Surf B Biointerfaces*. 2009; 73(1):51–57.
46. Suliman Y AO, Ali D, Alarifi S, Harrath AH, Mansour L, Alwasel SH. Evaluation of cytotoxic, oxidative stress, proinflammatory and genotoxic effect of silver nanoparticles in human lung epithelial cells. *Environ Toxicol*. Epub 2013 Jun 26.
47. Kim S, Ryu DY. Silver nanoparticle-induced oxidative stress, genotoxicity and apoptosis in cultured cells and animal tissues. *J Appl Toxicol*. 2013;33(2):78–89.
48. Edetsberger M, Gaubitzer E, Valic E, Waigmann E, Köhler G. Detection of nanometer-sized particles in living cells using modern fluorescence fluctuation methods. *Biochem Biophys Res Commun*. 2005;332(1):109–116.
49. Jiang H, Wang C, Guo Z, Wang Z, Liu L. Silver nanocrystals mediated combination therapy of radiation with magnetic hyperthermia on glioma cells. *J Nanosci Nanotechnol*. 2012;12(11):8276–8281.
50. Mukherjee D, Botelho D, Gow AJ, Zhang J, Georgopoulos PG. Computational multiscale toxicodynamic modeling of silver and carbon nanoparticle effects on mouse lung function. *PLoS One*. 2013;8(12): e80917.
51. van der Zande M, Vandebriel RJ, Van Doren E, et al. Distribution, elimination, and toxicity of silver nanoparticles and silver ions in rats after 28-day oral exposure. *ACS Nano*. 2012;6(8):7427–7442.
52. Shi J, Sun X, Lin Y, et al. Endothelial cell injury and dysfunction induced by silver nanoparticles through oxidative stress via IKK/NF-κB pathways. *Biomaterials*. 2014;35(24):6657–6666.
53. Lee YH, Cheng FY, Chiu HW, et al. Cytotoxicity, oxidative stress, apoptosis and the autophagic effects of silver nanoparticles in mouse embryonic fibroblasts. *Biomaterials*. 2014;35(16): 4706–4715.
54. Sambaziotis D, Kapranos N, Kontogeorgos G. Correlation of bcl-2 and bax with apoptosis in human pituitary adenomas. *Pituitary.* 2003;6(3):127–133.
55. Park MV, Neigh AM, Vermeulen JP, et al. The effect of particle size on the cytotoxicity, inflammation, developmental toxicity and genotoxicity of silver nanoparticles. *Biomaterials*. 2011;32(36):9810–9817.
56. Chan FK, Moriwaki K, De Rosa MJ. Detection of necrosis by release of lactate dehydrogenase activity. *Methods Mol Biol*. 2013;979: 65–70.
57. Wajant H, Scheurich P. Tumor necrosis factor receptor-associated factor (TRAF) 2 and its role in TNF signaling. *Int J Biochem Cell Biol*. 2001; 33(1):19–32.
58. Grell M, Zimmermann G, Hülser D, Pfizenmaier K, Scheurich P. TNF receptors TR60 and TR80 can mediate apoptosis via induction of distinct signal pathways. *J Immunol*. 1994;153(5):1963–1972.
59. Haranaka K, Satomi N. Cytotoxic activity of tumor necrosis factor (TNF) on human cancer cells in vitro. *Jpn J Exp Med*. 1981;51(3): 191–194.
60. Voelkel-Johnson C, Entingh AJ, Wold WS, Gooding LR, Laster SM. Activation of intracellular proteases is an early event in TNF-induced apoptosis. *J Immunol*. 1995;154(4):1707–1716.

61. Miura N, Shinohara Y. Cytotoxic effect and apoptosis induction by silver nanoparticles in HeLa cells. *Biochem Biophys Res Commun*. 2009; 390(3):733–737.
62. Kim TH, Kim M, Park HS, Shin US, Gong MS, Kim HW. Size-dependent cellular toxicity of silver nanoparticles. *J Biomed Mater Res A*. 2012;100(4):1033–1043.
63. Carlson C, Hussain SM, Schrand AM, et al. Unique cellular interaction of silver nanoparticles: size-dependent generation of reactive oxygen species. *J Phys Chem B*. 2008;112(43):13608–13619.
64. Kim S, Choi JE, Choi J, et al. Oxidative stress-dependent toxicity of silver nanoparticles in human hepatoma cells. *Toxicol In Vitro*. 2009; 23(6):1076–1084.
65. Foldbjerg R, Olesen P, Hougaard M, Dang DA, Hoffmann HJ, Autrup H. PVP-coated silver nanoparticles and silver ions induce reactive oxygen species, apoptosis and necrosis in THP-1 monocytes. *Toxicol Lett*. 2009;190(2):156–162.
66. Franco-Molina MA, Mendoza-Gamboa E, Sierra-Rivera CA, et al. Antitumor activity of colloidal silver on MCF-7 human breast cancer cells. *J Exp Clin Cancer Res*. 2010;29:148.
67. Dayem AA, Kim B, Gurunathan S, et al. Biologically synthesized silver nanoparticles induce neuronal differentiation of SH-SY5Y cells via modulation of reactive oxygen species, phosphatases, and kinase signaling pathways. *Biotechnol J*. 2014;9(7):934–943.
68. Braydich-Stolle LK, Lucas B, Schrand A, et al. Silver nanoparticles disrupt GDNF/Fyn kinase signaling in spermatogonial stem cells. *Toxicol Sci*. 2010;116(2):577–589.
69. Franco JL, Posser T, Dunkley PR, et al. Methylmercury neurotoxicity is associated with inhibition of the antioxidant enzyme glutathione peroxidase. *Free Radic Biol Med*. 2009;47(4):449–457.
70. Inkielewicz-Stepniak I, Santos-Martinez MJ, Medina C, Radomski MW. Pharmacological and toxicological effects of co-exposure of human gingival fibroblasts to silver nanoparticles and sodium fluoride. *Int J Nanomedicine*. 2014;9:1677–1687.
71. Ramírez-Lee MA, Rosas-Hernández H, Salazar-García S, et al. Silver nanoparticles induce anti-proliferative effects on airway smooth muscle cells. Role of nitric oxide and muscarinic receptor signaling pathway. *Toxicol Lett*. 2014;224(2):246–256.
72. Miethling-Graff R, Rumpker R, Richter M, et al. Exposure to silver nanoparticles induces size- and dose-dependent oxidative stress and cytotoxicity in human colon carcinoma cells. *Toxicol In Vitro*. 2014;28(7): 1280–1289.
73. Mizushima N. Autophagy. *FEBS Lett*. 2010;584(7):1279.
74. Zabirnyk O, Yezhelyev M, Seleverstov O. Nanoparticles as a novel class of autophagy activators. *Autophagy*. 2007;3(3):278–281.
75. Yamawaki H, Iwai N. Cytotoxicity of water-soluble fullerene in vascular endothelial cells. *Am J Physiol Cell Physiol*. 2006;290(6): C1495–C1502.
76. Johnson-Lyles DN, Peifley K, Lockett S, et al. Fullerenol cytotoxicity in kidney cells is associated with cytoskeleton disruption, autophagic vacuole accumulation, and mitochondrial dysfunction. *Toxicol Appl Pharmacol*. 2010;248(3):249–258.
77. Stern ST, Zolnik BS, McLeland CB, Clogston J, Zheng J, McNeil SE. Induction of autophagy in porcine kidney cells by quantum dots: a common cellular response to nanomaterials? *Toxicol Sci*. 2008;106(1): 140–152.
78. Griffiths GM. Gaucher disease: forging a new path to the lysosome. *Cell*. 2007;131(4):647–649.
79. Li JJ, Hartono D, Ong CN, Bay BH, Yung LY. Autophagy and oxidative stress associated with gold nanoparticles. *Biomaterials*. 2010;31(23):5996–6003.
80. Chen Y, McMillan-Ward E, Kong J, Israels SJ, Gibson SB. Oxidative stress induces autophagic cell death independent of apoptosis in transformed and cancer cells. *Cell Death Differ*. 2008;15(1):171–182.
81. Moore MN. Autophagy as a second level protective process in conferring resistance to environmentally-induced oxidative stress. *Autophagy*. 2008;4(2):254–256.
82. Huang Q, Shen HM. To die or to live: the dual role of poly(ADP-ribose) polymerase-1 in autophagy and necrosis under oxidative stress and DNA damage. *Autophagy*. 2009;5(2):273–276.
83. Funnell WR, Maysinger D. Three-dimensional reconstruction of cell nuclei, internalized quantum dots and sites of lipid peroxidation. *J Nanobiotechnology*. 2006;4:10.
84. Jin Z, El-Deiry WS. Overview of cell death signaling pathways. *Cancer Biol Ther*. 2005;4(2):139–163.
85. Eom HJ, Choi J. p38 MAPK activation, DNA damage, cell cycle arrest and apoptosis as mechanisms of toxicity of silver nanoparticles in Jurkat T cells. *Environ Sci Technol*. 2010;44(21):8337–8342.
86. Satapathy SR, Mohapatra P, Preet R, et al. Silver-based nanoparticles induce apoptosis in human colon cancer cells mediated through p53. *Nanomedicine (Lond)*. 2013;8(8):1307–1322.
87. Foldbjerg R, Irving ES, Hayashi Y, et al. Global gene expression profiling of human lung epithelial cells after exposure to nanosilver. *Toxicol Sci*. 2012;130(1):145–157.
88. Chai F, Evdokiou A, Young GP, Zalewski PD. Involvement of p21(Waf1/Cip1) and its cleavage by DEVD-caspase during apoptosis of colorectal cancer cells induced by butyrate. *Carcinogenesis*. 2000; 21(1):7–14.
89. Kasibhatla S, Tseng B. Why target apoptosis in cancer treatment? *Mol Cancer Ther*. 2003;2(6):573–580.
90. Wang J, Green PS, Simpkins JW. Estradiol protects against ATP depletion, mitochondrial membrane potential decline and the generation of reactive oxygen species induced by 3-nitroproprionic acid in SK-N-SH human neuroblastoma cells. *J Neurochem*. 2001;77(3):804–811.
91. Govender R, Phulukdaree A, Gengan RM, Anand K, Chuturgoon AA. Silver nanoparticles of Albizia adianthifolia: the induction of apoptosis in human lung carcinoma cell line. *J Nanobiotechnology*. 2013;11:5.
92. Yuan L, Lu CL, Wang Y, Li Y, Li XY. Ang (1–7) protects islet endothelial cells from palmitate-induced apoptosis by AKT, eNOS, p38 MAPK, and JNK pathways. *J Diabetes Res*. 2014;2014: 391476.
93. Gao J, Gao J, Qian L, et al. Activation of p38-MAPK by CXCL4/CXCR3 axis contributes to p53-dependent intestinal apoptosis initiated by 5-fluorouracil. *Cancer Biol Ther*. 2014;15(8):982–991.
94. Valko M, Rhodes CJ, Moncol J, Izakovic M, Mazur M. Free radicals, metals and antioxidants in oxidative stress-induced cancer. *Chem Biol Interact*. 2006;160(1):1–40.
95. Jackson SP, Bartek J. The DNA-damage response in human biology and disease. *Nature*. 2009;461(7267):1071–1078.
96. Ahamed M, Siddiqui MA, Akhtar MJ, Ahmad I, Pant AB, Alhadlaq HA. Genotoxic potential of copper oxide nanoparticles in human lung epithelial cells. *Biochem Biophys Res Commun*. 2010;396(2): 578–583.
97. Sur I, Altunbek M, Kahraman M, Culha M. The influence of the surface chemistry of silver nanoparticles on cell death. *Nanotechnology*. 2012;23(37):375102.
98. Raucci F, D'Aniello A, Di Fiore MM. Stimulation of androgen production by D-aspartate through the enhancement of StAR, P450scc and 3β-HSD mRNA levels in vivo rat testis and in culture of immature rat Leydig cells. *Steroids*. 2014;84:103–110.
99. Payne AH, Youngblood GL. Regulation of expression of steroidogenic enzymes in Leydig cells. *Biol Reprod*. 1995;52(2):217–225.
100. Payne AH, Hales DB. Overview of steroidogenic enzymes in the pathway from cholesterol to active steroid hormones. *Endocr Rev*. 2004; 25(6):947–970.
101. Stocco DM, Clark BJ. Role of the steroidogenic acute regulatory protein (StAR) in steroidogenesis. *Biochem Pharmacol*. 1996;51(3): 197–205.
102. Gudermann T, Birnbaumer M, Birnbaumer L. Evidence for dual coupling of the murine luteinizing hormone receptor to adenylyl cyclase and phosphoinositide breakdown and Ca^{2+} mobilization. Studies with the cloned murine luteinizing hormone receptor expressed in L cells. *J Biol Chem*. 1992;267(7):4479–4488.

103. Stocco DM, Clark BJ. Regulation of the acute production of steroids in steroidogenic cells. *Endocr Rev*. 1996;17(3):221–244.
104. Walsh LP, Stocco DM. Effects of lindane on steroidogenesis and steroidogenic acute regulatory protein expression. *Biol Reprod*. 2000; 63(4):1024–1033.
105. Clewell RA, Campbell JL, Ross SM, Gaido KW, Clewell HJ, Andersen ME. Assessing the relevance of in vitro measures of phthalate inhibition of steroidogenesis for in vivo response. *Toxicol In Vitro*. 2010;24(1):327–334.
106. Feng Y, Fang X, Shi Z, Xu M, Dai J. Effects of PFNA exposure on expression of junction-associated molecules and secretory function in rat Sertoli cells. *Reprod Toxicol*. 2010;30(3):429–437.
107. Wu J, Zhang Y, Tian GG, et al. Short-type PB-cadherin promotes self-renewal of spermatogonial stem cells via multiple signaling pathways. *Cell Signal*. 2008;20(6):1052–1060.
108. Zhang X, Shi K, Li Y, Zhang H, Hao J. Lipopolysaccharide inhibits the self-renewal of spermatogonial stem cells in vitro via downregulation of GDNF expression in Sertoli cells. *Reprod Toxicol*. 2014; 45:87–93.
109. Qiu L, Zhang X, Zhang X, et al. Sertoli cell is a potential target for perfluorooctane sulfonate-induced reproductive dysfunction in male mice. *Toxicol Sci*. 2013;135(1):229–240.
110. Lui WY, Lee WM, Cheng CY. TGF-betas: their role in testicular function and Sertoli cell tight junction dynamics. *Int J Androl*. 2003; 26(3):147–160.
111. Cheng CY, Wong EW, Lie PP, et al. Environmental toxicants and male reproductive function. *Spermatogenesis*. 2011;1(1):2–13.
112. Ryu BY, Orwig KE, Kubota H, Avarbock MR, Brinster RL. Phenotypic and functional characteristics of spermatogonial stem cells in rats. *Dev Biol*. 2004;274(1):158–170.
113. Wang J, Cao H, Xue X, et al. Effect of vitamin C on growth of caprine spermatogonial stem cells in vitro. *Theriogenology*. 2014;81(4): 545–555.
114. Baazm M, Abolhassani F, Abbasi M, Habibi Roudkenar M, Amidi F, Beyer C. An improved protocol for isolation and culturing of mouse spermatogonial stem cells. *Cell Reprogram*. 2013;15(4):329–336.
115. Hofmann MC. Gdnf signaling pathways within the mammalian spermatogonial stem cell niche. *Mol Cell Endocrinol*. 2008;288(1–2): 95–103.
116. Hai Y, Hou J, Liu Y, et al. The roles and regulation of Sertoli cells in fate determinations of spermatogonial stem cells and spermatogenesis. *Semin Cell Dev Biol*. 2014;29:66–75.
117. Simon L, Ekman GC, Tyagi G, Hess RA, Murphy KM, Cooke PS. Common and distinct factors regulate expression of mRNA for ETV5 and GDNF, Sertoli cell proteins essential for spermatogonial stem cell maintenance. *Exp Cell Res*. 2007;313(14):3090–3099.